

## Studies on the Dynamics of Saltation in Drifting Snow

By

**Kenji KOSUGI\***, **Kouichi NISHIMURA\*\*** and **Norikazu MAENO\*\***

*\*Shinjo Branch of Snow and Ice Studies, National Research Institute  
for Earth Science and Disaster Prevention*

*\*\*Institute of Low Temperature Science, Hokkaido University*

### Abstract

Saltation is one of the most fundamental processes in transporting snow particles in drifting or blowing snow. The statistical saltation process was investigated by studying the collision characteristics of ice spheres (diameter 2.8 mm) impacting on a granular bed composed of identical ice particles. Rebound velocities and angles of ice particles were measured as functions of the incident velocity and angle at a temperature of  $-18^{\circ}\text{C}$ , and the vertical restitution coefficient ( $e_v$ ), defined as the vertical component of a rebound velocity divided by that of the incident velocity, was estimated.

The average vertical restitution coefficient decreased with the increase of the incident angle due to the increasing interaction with lying particles. On the other hand, this coefficient was almost independent of the incident velocity. The impact of a single ice particle often gave rise to the ejection or splash of other particles, the number of which sometimes amounted to six.

The statistical behavior of the saltation or splash process can be described by splash functions:  $S_v(e_v)$ ,  $S_h(e_h)$  and  $S_e(n_e)$ , where  $e_v$ ,  $e_h$  and  $n_e$  are the vertical restitution coefficient, the horizontal restitution coefficient and the number of ejected particles, respectively. Each of the splash functions represents the probability of the occurrence of each physical quantity. In the study the splash function  $S_v(e_v)$  was determined as follows:

$$S_v(e_v; \theta, V_i) = [1/\beta\Gamma(\alpha)](e_v/\beta)^{\alpha-1}\exp(-e_v/\beta)$$

where  $\theta$  and  $V_i$  are the incident angle and velocity, respectively,  $\Gamma(\alpha)$  is the gamma function,  $\alpha$  is the shape parameter ( $\alpha = 0.056\theta + 3.8$ ), and  $\beta$  is the scale parameter ( $\beta = 4.9\theta^{-1.3}$ ). The result shows that the splash function in the vertical motion is only dependent on the incident angle and not on the incident velocity in the range investigated in the present study (3.5-10 m/s).

Wind-tunnel and numerical experiments of saltation were carried out to obtain the vertical profiles of ice particle concentration. The identical ice particles used in the collision experiments were also used in the wind-tunnel experiments. In the numerical experiments, the splash function derived from the collision experiments was applied to determine the rebound velocity of saltating ice particles. Both the results of the two

---

\*Second Laboratory, National Institute Postdoctoral Fellow

saltation experiments showed an exponential decrease of the particle concentration with increasing height. These results characterize the mass transport by saltation in the saltation layer.

**Key words** : drifting snow, saltation, restitution coefficient, impact experiments, splash function

## 1. Introduction

In drifting or blowing snow, wind transports snow particles in three types of motion : creep, saltation and suspension. Creep is the migration of snow particles along the surface of a snow cover. Saltation is the successive jumping on the snow surface. Saltating particles compose a so-called saltation layer. Above the saltation layer, snow particles are held in suspension by the turbulence of wind.

Saltation is the most fundamental and the most important process among the three types of motion for the following reasons. Saltation affords the largest part of the total mass transport of drifting snow (Kobayashi, 1972). Creep soon develops into saltation and the suspension begins from saltation. In spite of the essential importance of the saltation process, however, physical mechanisms responsible for it have not been well understood yet.

Recent numerical simulations of sand storms and drifting snow processes are useful and effective in many practical applications. An example of the applications is to estimate the following: the formation of dunes, the maximum transport of snow by realistic wind, and probable formation of snow drifts around structures such as houses, bridges, roads, as well as other places (e.g. Irwin, 1983; Wipperman and Gross, 1985; Pomeroy and Male, 1986; Uematsu *et al.*, 1989). However, all these simulation models depend definitely on various assumptions made on the physical processes taking place in drifting snow, especially those in the saltation layer. At present it is impossible to take into account in models the detailed physical process of snow particle collision and saltation on the snow surface. It is, however, vital in improving the general applicability of various practical computer models and in linking them with more realistic physical understanding of saltation processes.

The basic mechanics of saltation were extensively investigated by Bagnold (1941) in his pioneering work on aeolian sand storms. Most of his findings are essentially applicable to snow particle saltation as manifested in natural drifting snow by Dyunin (1954, 1963), Budd *et al.* (1966), Kobayashi (1972) and others. Wind-tunnel studies of snow particle saltation in drifting snow were made by Kikuchi (1981), Araoka and Maeno

(1981) and Maeno *et al.* (1985). Many results of the above studies have led to the general understanding of the drifting or blowing snow phenomenon and the useful empirical relations for mass transport rates, vertical concentration profiles and others.

In their wind-tunnel experiments of saltating snow particles, Araoka and Maeno (1981) recognized that the angle and velocity of an incident snow particle and those of rebounding ones are not unique but distributed in wide ranges. At a mean wind speed of 5 m/s (25 cm above the snow surface) and a temperature of  $-9^{\circ}\text{C}$ , they showed that incidence and lift-off (rebound) angles measured from the horizontal plane are distributed in ranges of 5 - 40 and 10 - 115 degrees, respectively. The much larger distribution of the latter angle is attributed to irregular collisions on a non-uniform snow surface. They also showed that the incident and rebound velocities are distributed. They emphasized the importance of detailed studies of the statistical nature of the collision or splash process on snow surfaces to obtain a more realistic understanding of the physics of the saltation phenomenon.

Recently similar results of distributed angles and larger rebound angles than incident angles were recognized in wind-tunnel measurements of sand and other granular materials (Willettts and Rice, 1985; Mitha *et al.*, 1986), and some efforts were made to find a numerical relation describing the splash process. Anderson and Haff (1988) tried to perform two-dimensional numerical simulations of particle impacts into a granular bed composed of identical spheres to get a quantitative description of the splash process. However, the physical interaction between particles must be characterized by the restitution coefficient, friction coefficient and elastic modulus, and it is clearly difficult to reasonably determine all the three parameters. It simply suggests the importance of conducting a systematic physical experiment of the splash process.

The purpose of the present paper is to find a quantitative relation that describes the statistical behavior of rebounding particles as a function of the incident velocity and angle. To get such an equation, that is a so-called splash function, we carried out a systematic experiment of ice particle collision on a surface composed of similar ice particles. Details of the splash experiments of ice particles are described in Chapter 2. Chapter 3 gives the procedure and results of a wind-tunnel experiment made to obtain numerical data of ice particle saltation. Chapter 4 gives the numerical computation of ice particle saltation by using the splash function obtained and the comparison of the numerical results with those of the wind-tunnel experiment. A concluding summary of the results is found in Chapter 5. Throughout the present study special attention was paid

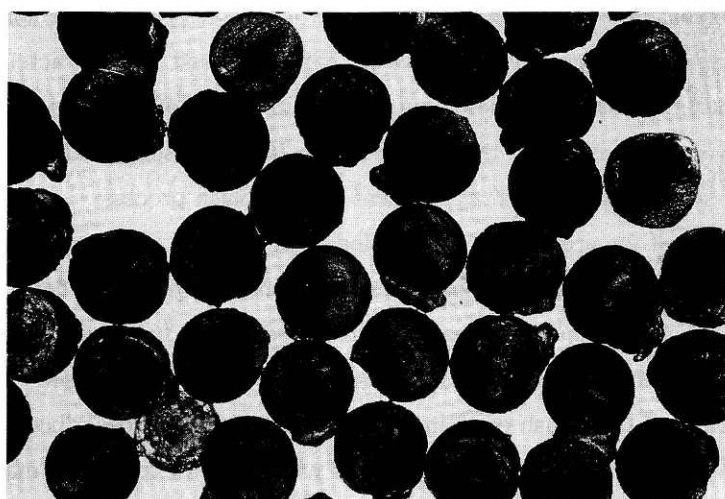
in the vertical motion of the ice particles because of its prime importance in the development of drifting snow in a realistic wind where the wind speed is usually larger at higher levels.

## 2. Splash experiments of ice particles

### 2.1 Apparatus and method of splash experiments

Ice particles used in the experiments were frozen droplets of distilled water which was dripped from an injector into a bath of liquid nitrogen to freeze into ice particles. Central parts of the ice particles thus obtained were opaque owing to the trapping of minute air bubbles. Nevertheless their bulk densities were larger than  $900 \text{ kg/m}^3$  and no specific effects of included bubbles could be noted in the splash experiment.

The ice particles were sieved to have a uniform size distribution. The sizes of the ice particles were measured in photographs as shown in **Photo 1**, and their size distribution is given in **Fig. 1**. The average of their diameters was 2.78 mm and the standard deviation was 0.08 mm; the coefficient of the variation was 2.9 %. The degree of sphericity of a particle was defined as the ratio of a perimeter of a circle with a projected area of the particle to that of its projection. The average degree of sphericity of the ice particles was 0.99, indicating that they can be regarded as spheres.



0 5mm

**Photo 1** Photograph of the ice particles.

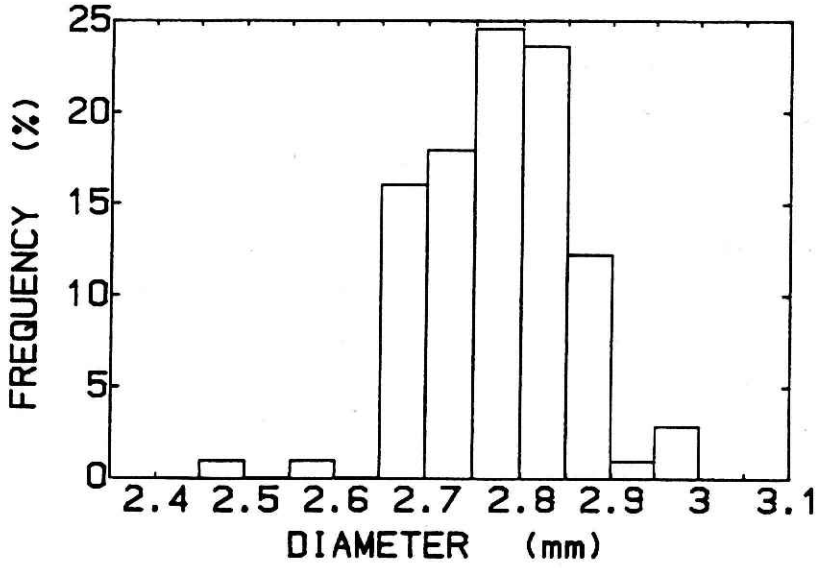


Fig. 1 Size distribution of the ice particles.

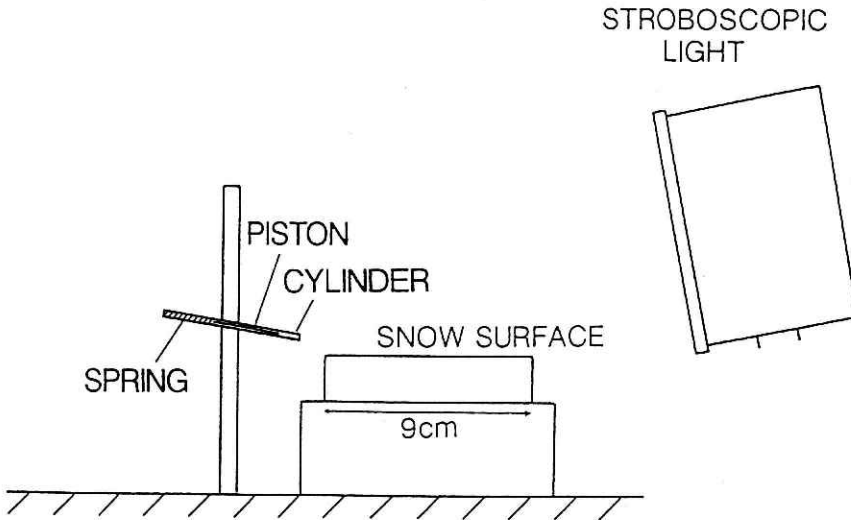


Fig. 2 Schematic drawing of the experimental apparatus.

**Fig. 2** gives a schematic drawing of the experimental apparatus of the splash experiment. The apparatus consisted of a container of ice particles and a gun shooting an ice particle. The container was a circular pan with 9 cm in diameter and 1.8 cm in height, which was set horizontally. Approximately 7,000 ice particles were packed in the container, and the surface of the ice particle bed was smoothed with a wooden plate. The particles were packed closely to give the maximum bulk density of roughly  $600 \text{ kg/m}^3$ , thus the particle bed consisting of six to seven layers of particles.

The gun was composed of a cylinder, a piston and a spring, and was pointed at the center of the container. Splash experiments were carried out in a range of the incidence speed from 3 m/s to 11 m/s and in a range of the incident angle from 5 degrees to 40 degrees measured from the horizontal.

Side views of the experimental set were recorded with a system of a video camera and a cassette recorder under stroboscopic illumination. The focal plane of the video camera was mostly in parallel with the plane of the incident motion of the ice particles. With the video system 60 frames were recorded every second and the frequency of the illumination was 400 Hz. Each frame then could record 6 or 7 illuminated images of an impacting and rebounding ice particle.

Velocities of the incidence and rebound of impacting particles were estimated from the video images as follows. The positions of an impacting particle were measured with a video x-y coordinator. The incidence and rebound velocities, which are defined as those of an impacting particle just before and after its collision with the bed, were estimated by the extrapolation of several successive approaching and lifting-off velocities. **Fig. 3** shows the notations of the velocities and angles.

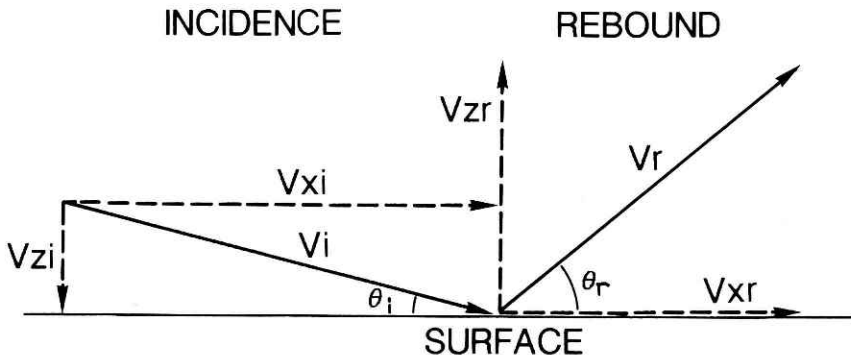


**Fig. 3** Notations of the velocities and angles.

All the experiments were conducted in a cold room maintained at a temperature of  $-18^{\circ}\text{C}$ .

## 2.2 Results of splash experiments of ice particles

### 2.2.1 General features of ice particle impact

**Photo 2** gives a series of pictures showing the impact process. An impacting ice particle rebounds off the surface of the bed composed of ice particles. The velocity of the impacting particle is reduced by the collision though the order of magnitude of its rebound velocity is usually the same. In the pictures of Photo 2 a few particles are ejected from the bed surface by the impact of a single particle. Velocities of the ejected particles are approximately two orders of magnitude smaller than those of the impacting particles. By the impact process particles around a collisional point are rearranged.

**Figs. 4, 5, 6 and 7** give the restitution coefficient ( $V_r/V_i$ , where  $V_r$  and  $V_i$  are the rebound and incident velocities, respectively) and the rebound angle ( $\theta_r$ ) plotted against the incident angle ( $\theta_i$ ) at the incident velocities of 3.5, 5.0, 7.5, and 10.0 m/s, respectively. At each incident velocity the restitution coefficient shows a wide distribution of measured values due to the irregular statistical impact with the rough bed surface. However, a clear decreasing tendency is noticed in average with the increasing incident angle. The observed maximum restitution coefficients at each incident angle correspond to the intrinsic restitution coefficient of ice colliding on a flat ice surface. The maximum value around 0.9 found in our results is in good agreement with that of Araoka and Maeno (1978). The decrease in the restitution coefficient with the increasing incident angle is attributed to the energy loss by the increased interaction with surrounding ice particles.

On the other hand, the distribution of the measured rebound angle in Figs. 4, 5, 6 and 7 gives no clear relations to the incident angle and velocities. However, the rebound angle has an important statistical relation to the restitution coefficient, which is explained below.

Next the measured restitution coefficient was plotted against the rebound angle at each incident angle and velocity in **Figs. 8, 9, 10 and 11**. Now it becomes clearer that at each incident velocity the restitution coefficient decreases with an increasing rebound angle in average and the distribution becomes larger with the increasing incident angle.

### 2.2.2 Ejection of bed particles

When an ice particle is impacting into the ice particle bed, it rebounds and the bed particles near the impact point are set into motion. Sometimes some of the bed particles are ejected off. The number of such ejected particles per impact,  $n_e$ , was measured and

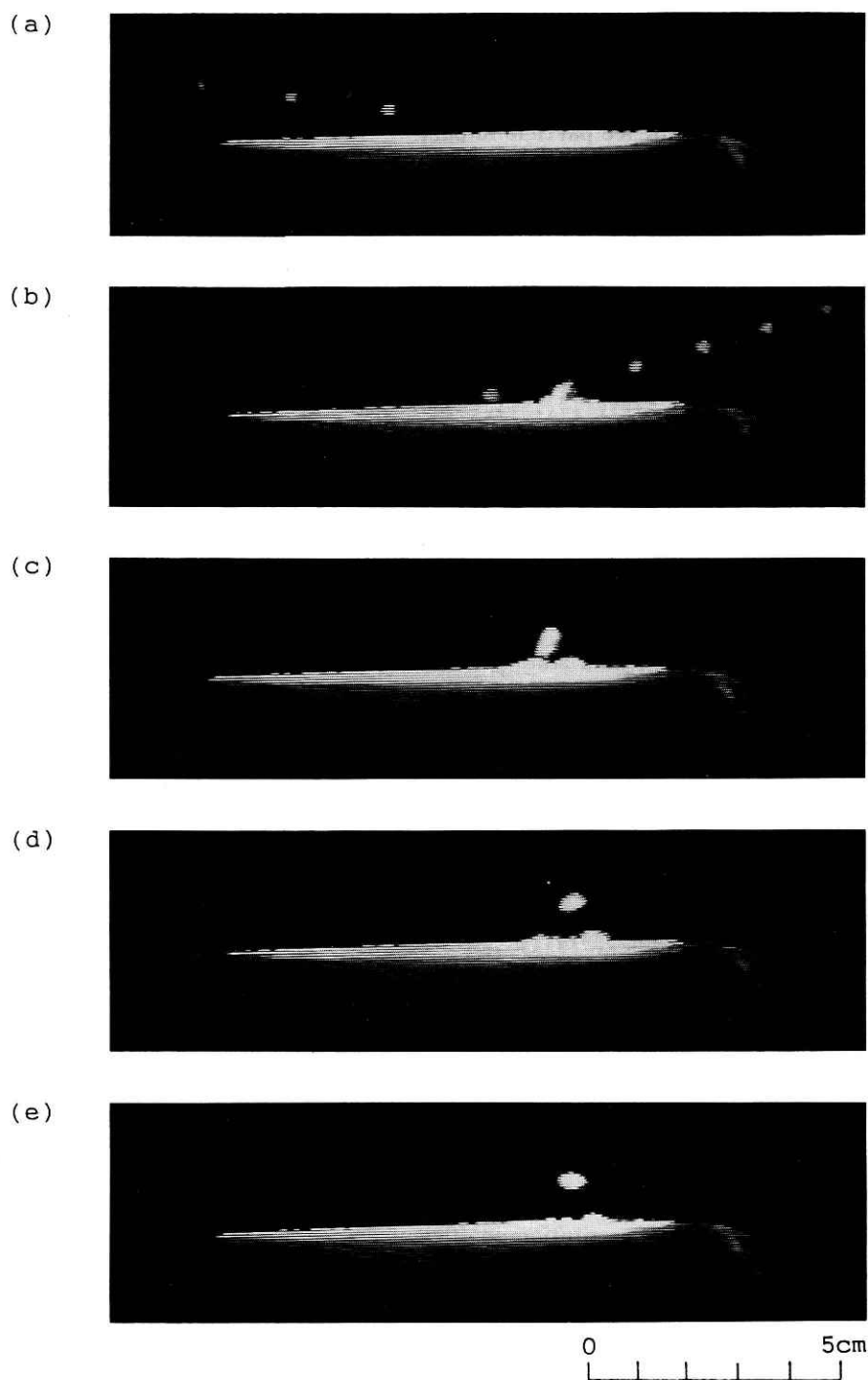


**Photo 2** A series of pictures showing the impact process.

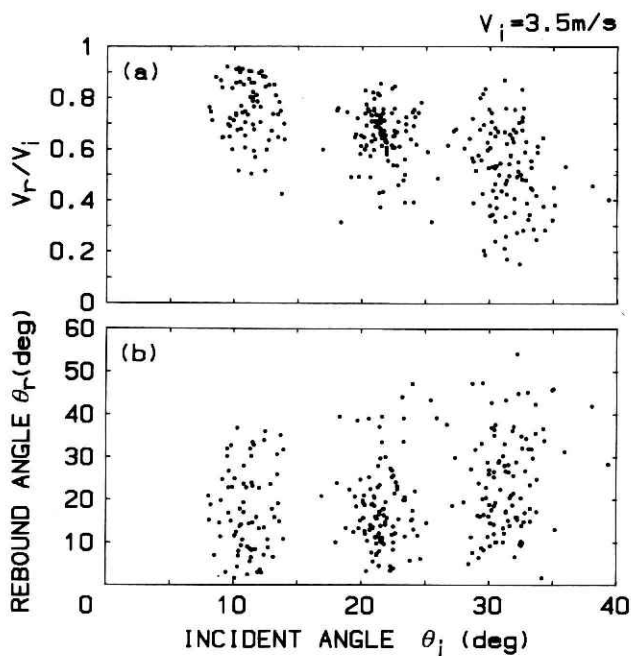


Fig. 4 Restitution coefficient (a) and rebound angle (b) plotted against the incident angle. Incident velocity is 3.5 m/s.

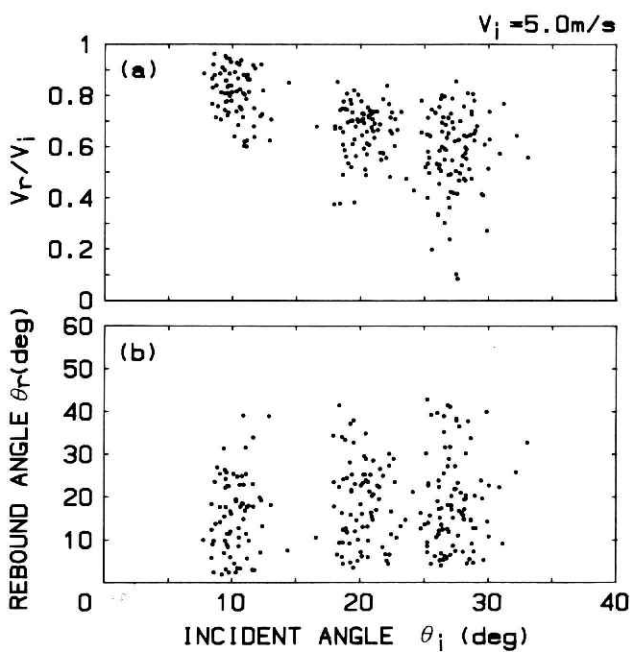


Fig. 5 Same as in Fig. 4 but for the incident velocity of 5.0 m/s.

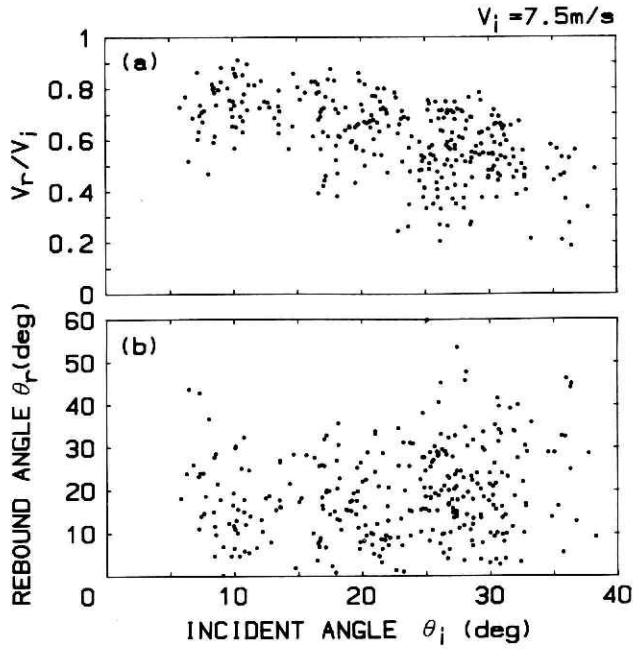


Fig. 6 Same as in Fig. 4 but for the incident velocity of 7.5 m/s.

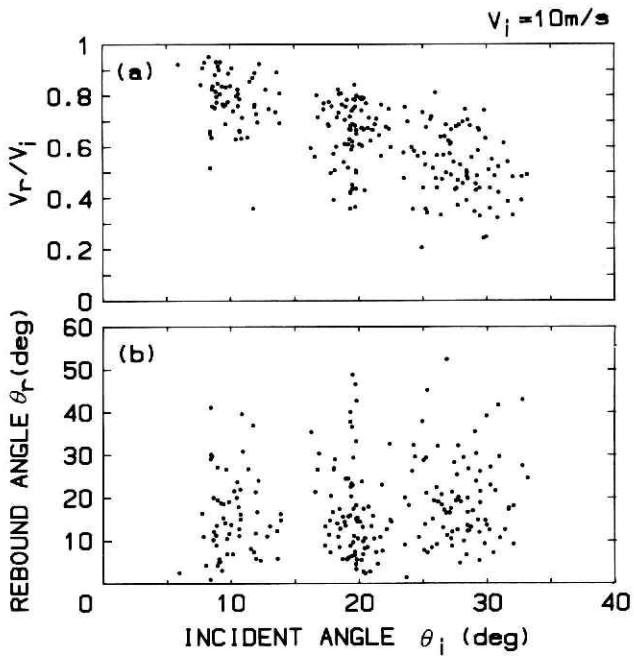
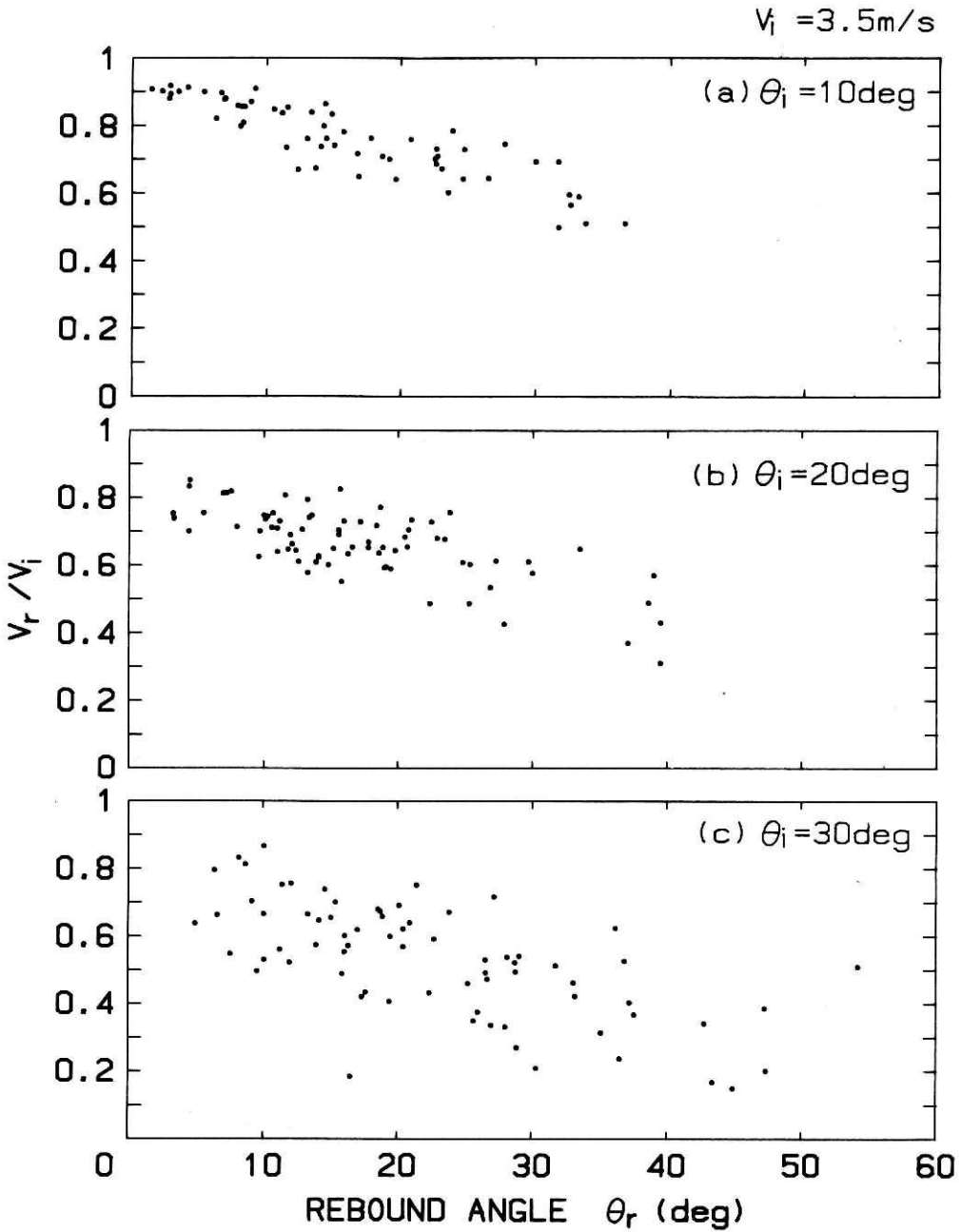


Fig. 7 Same as in Fig. 4 but for the incident velocity of 10 m/s.



**Fig. 8** Restitition coefficient plotted against the rebound angle at the incident angles of 10(a), 20(b) and 30(c) degrees. Incident velocity is 3.5 m/s.

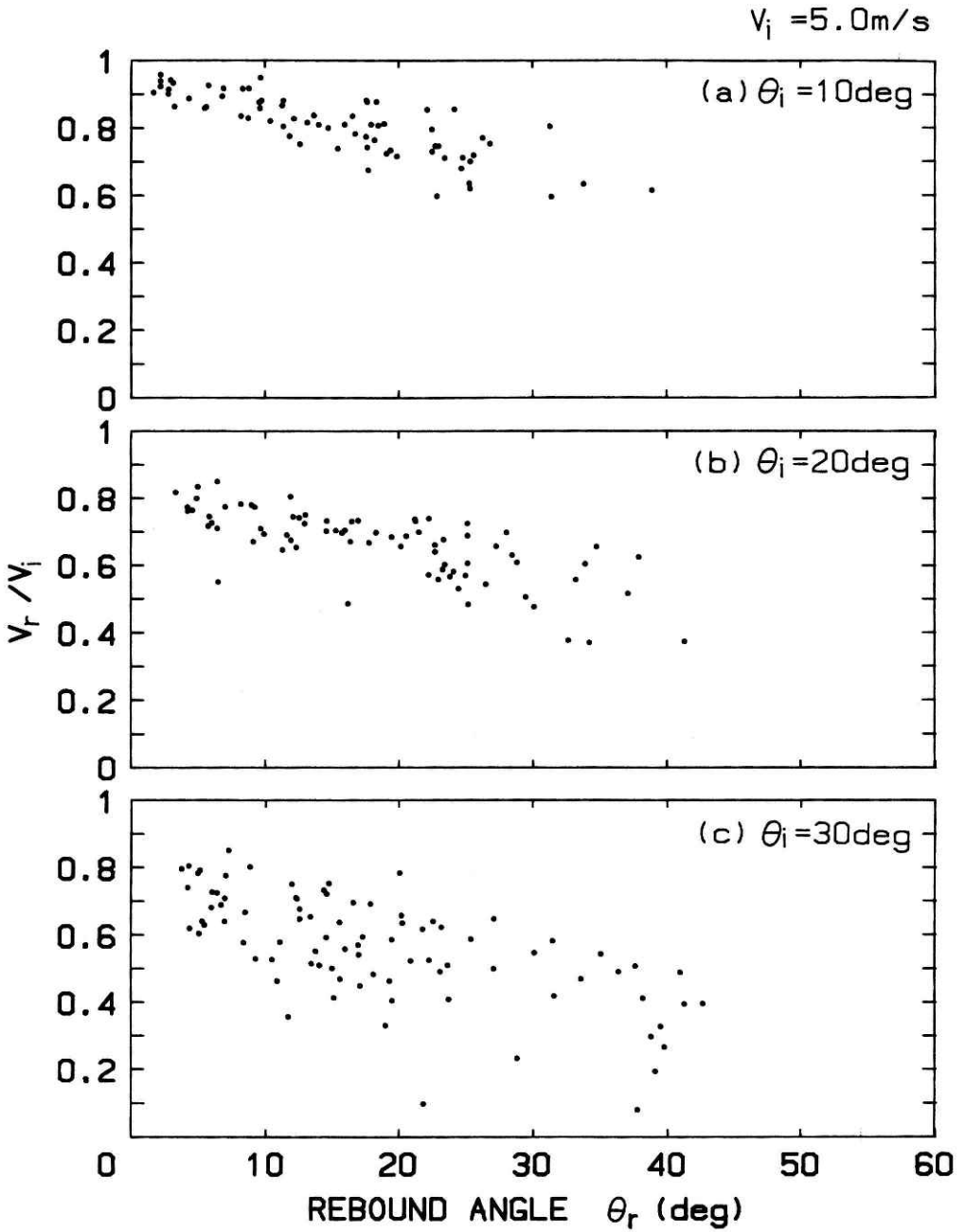


Fig. 9 Same as in Fig. 8 but for the incident velocity of 5.0 m/s.

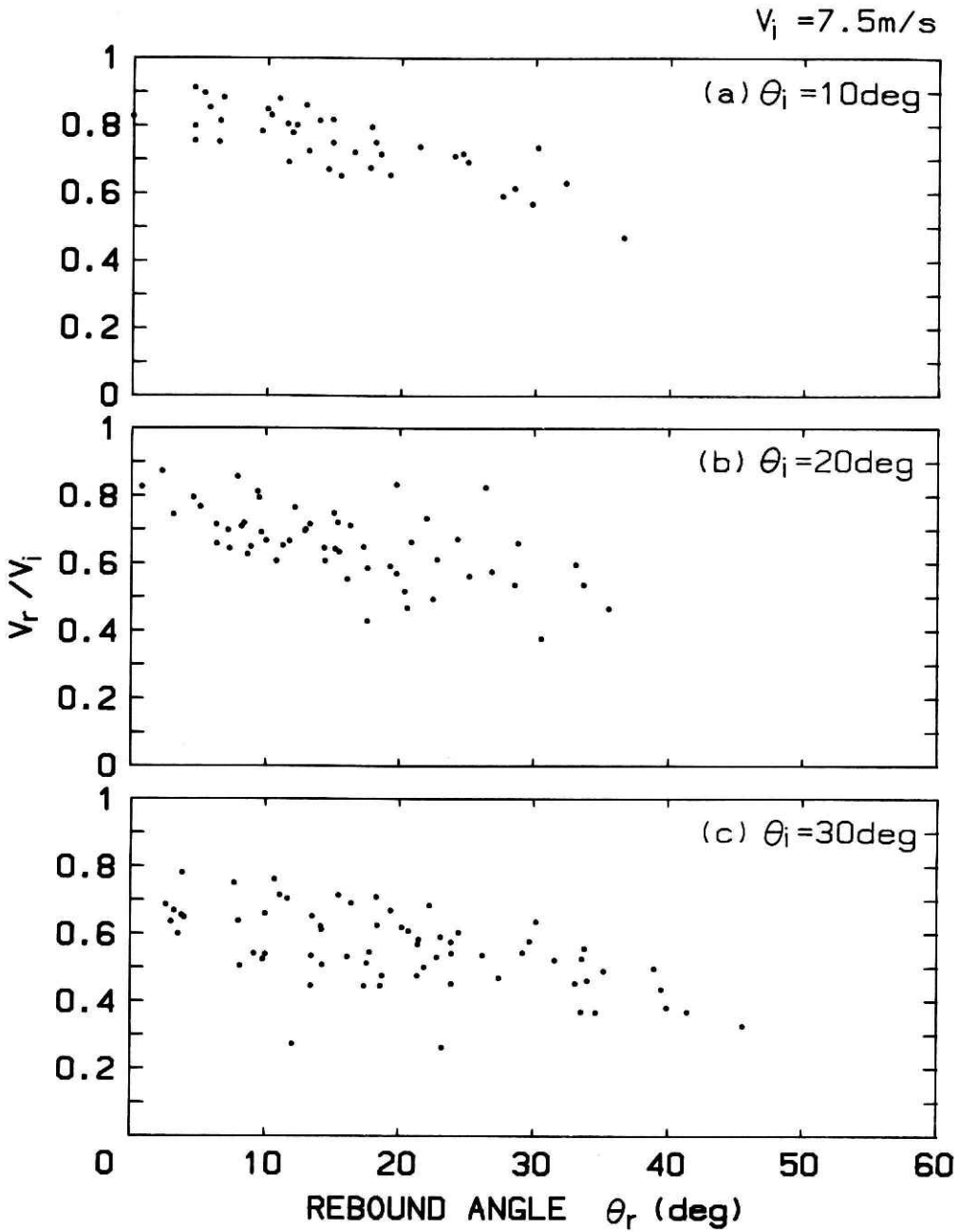


Fig. 10 Same as in Fig. 8 but for the incident velocity of 7.5 m/s.

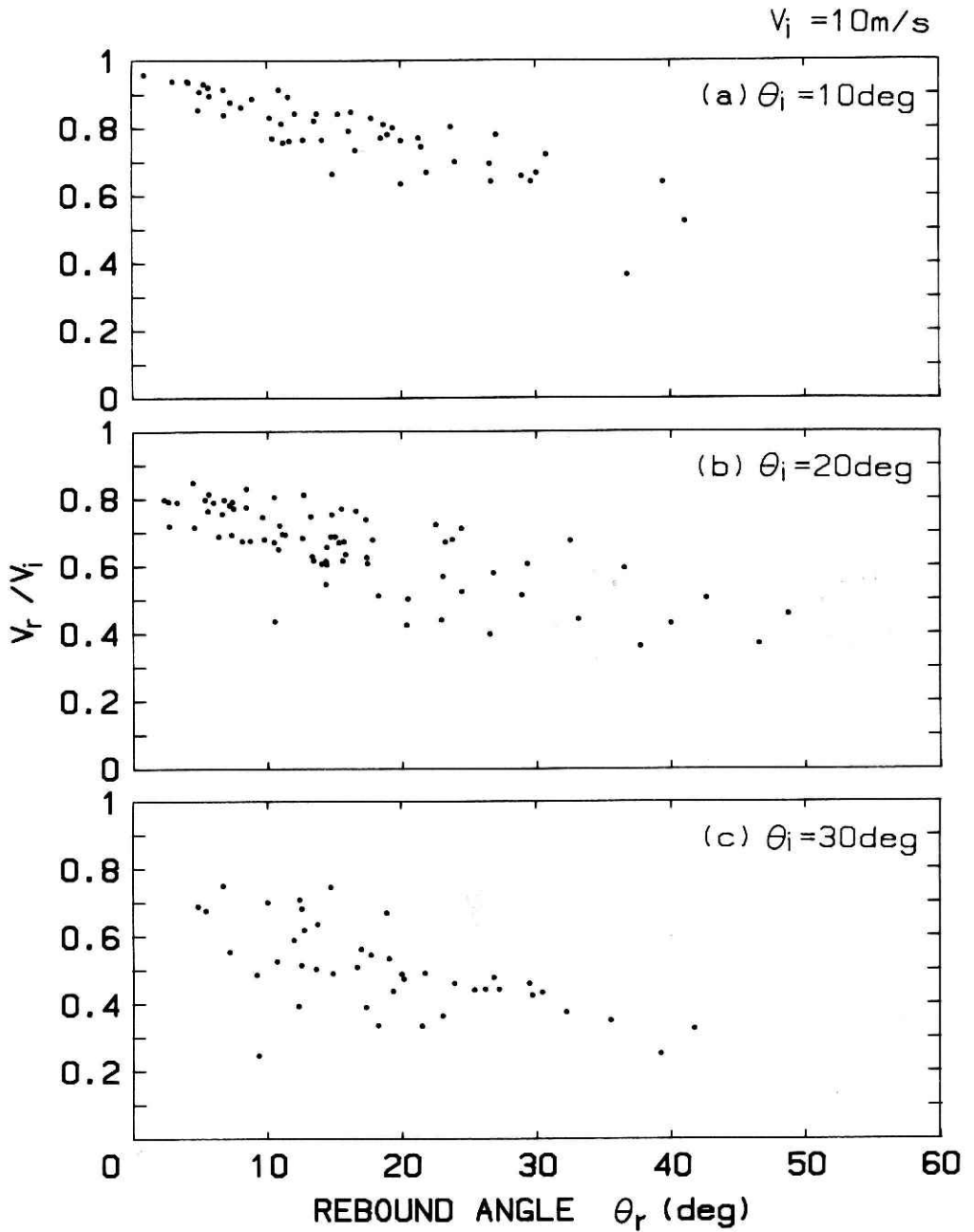
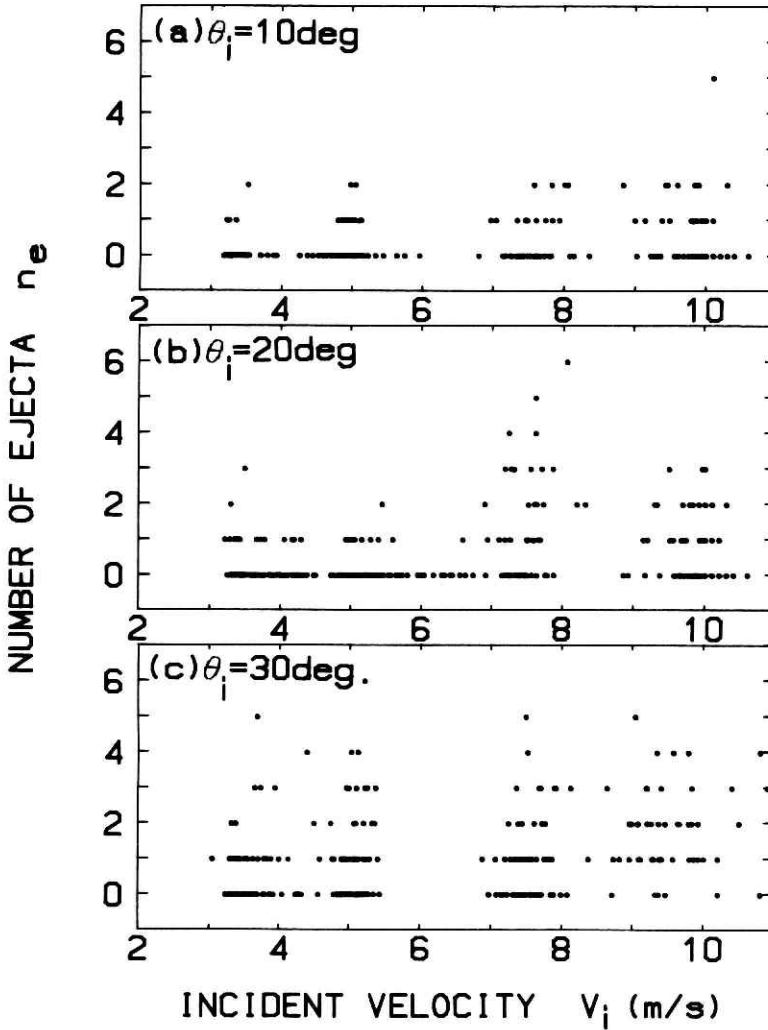


Fig. 11 Same as in Fig. 8 but for the incident velocity of 10 m/s.

plotted against the incident velocity, incident angle and rebound angle in **Figs. 12, 13** and **14**, respectively. It is clear in Figs. 12 and 13 that the number of ejected particles increases with an increasing incident angle and velocity and amounts to six particles per impact.



**Fig. 12** Number of ejected particles per impact plotted against the incident velocity. Incident angle : (a) 10 degrees, (b) 20 degrees, (c) 30 degrees.

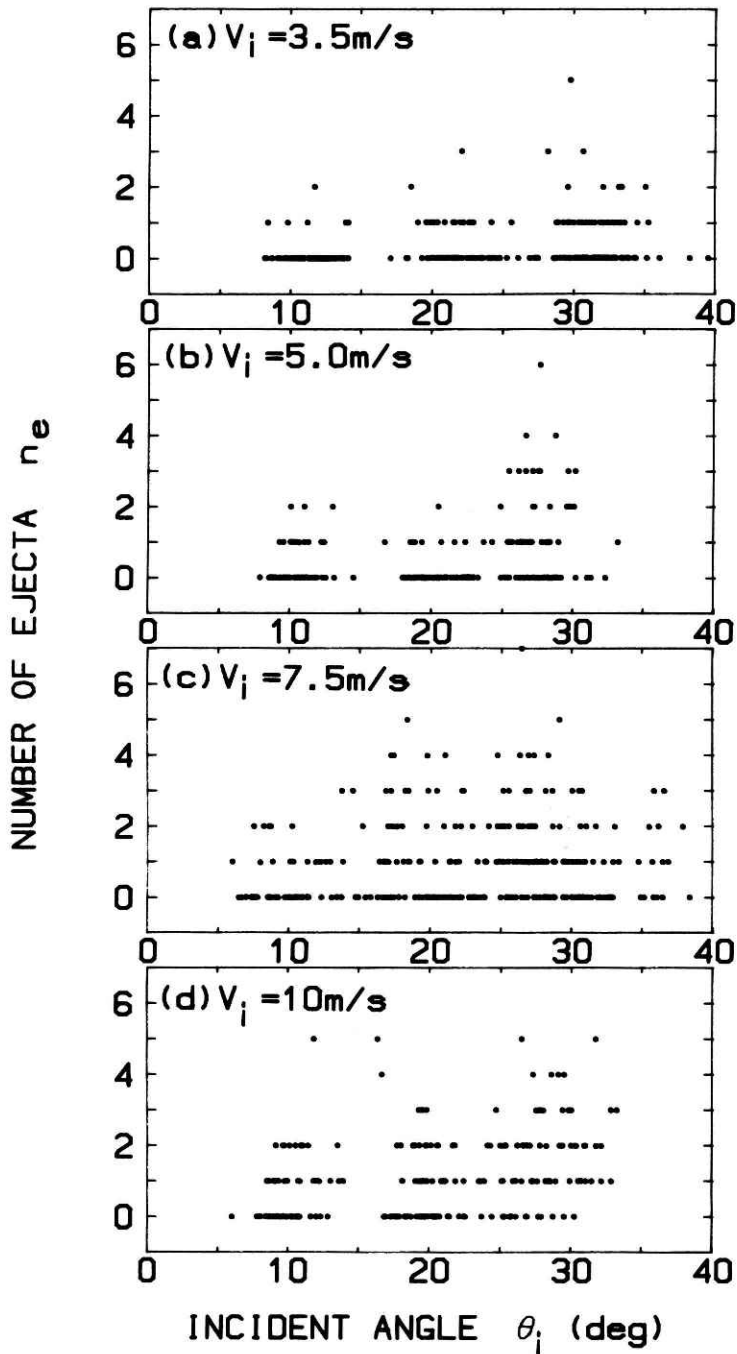
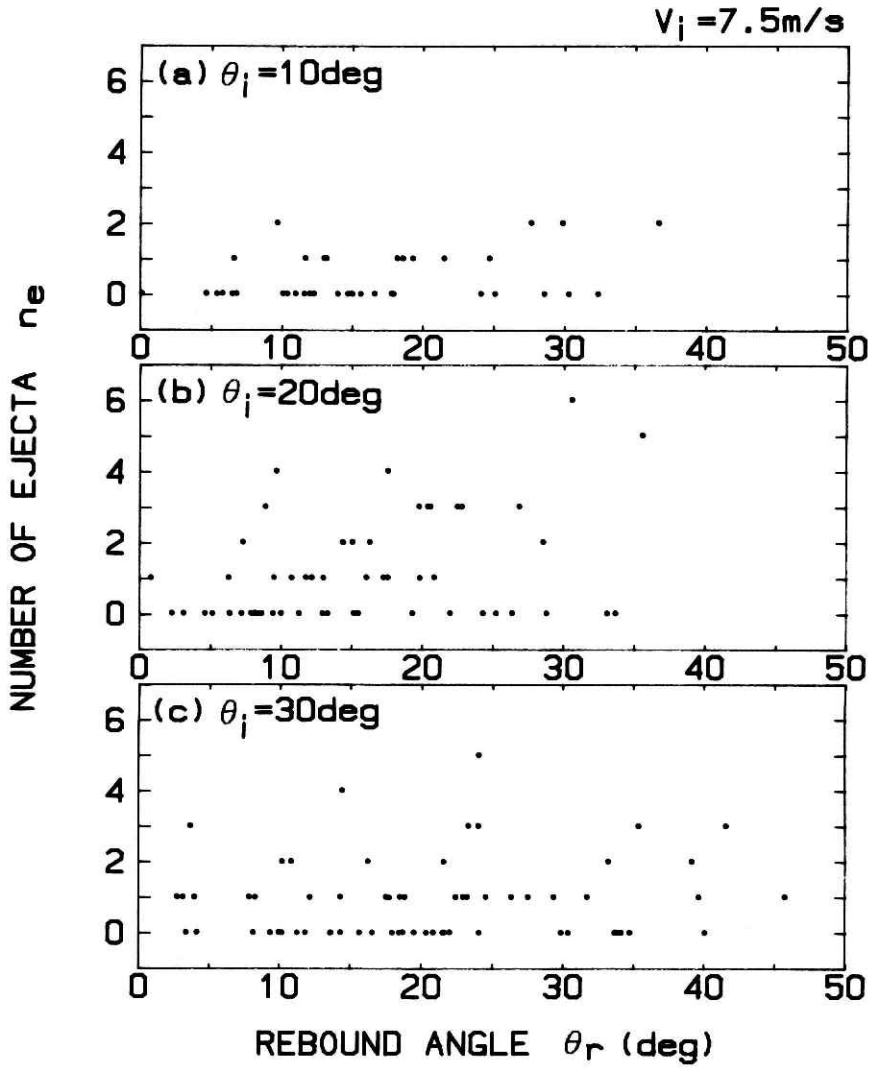


Fig. 13 Number of ejected particles per impact plotted against the incident angle.

Incident velocity : (a) 3.5 m/s, (b) 5.0 m/s, (c) 7.5 m/s, (d) 10 m/s.



**Fig. 14** Number of ejected particles per impact plotted against the rebound angle. Incident angle: (a) 10 degrees, (b) 20 degrees, (c) 30 degrees. Incident velocity is 7.5 m/s.

### 2.2.3 Vertical restitution coefficient of ice particles

**Figs. 15, 16, 17 and 18** show relations between the vertical and horizontal components of the measured rebound velocity at given incident velocities and angles, in which each component is normalized with the incident velocity. In each figure a straight line connecting a datum point and the origin gives a velocity vector describing the rebound motion. It is clearly shown that shorter vectors appear as the incident angle increases. Even more important is the fact that more data points appear above each straight line as the incident angle decreases. This means that an ice particle tends to lift up even higher than before the impact when the incident angle is small. The physical situation can be adequately described with the following two restitution coefficients.

The vertical and horizontal restitution coefficients are defined respectively as follows:

$$e_v = V_{zr} / V_{zi} \quad (1)$$

and

$$e_h = V_{xr} / V_{xi}, \quad (2)$$

where  $V_{zr}$  and  $V_{xr}$  are the vertical and horizontal components of the rebound velocity, and  $V_{zi}$  and  $V_{xi}$  are the vertical and horizontal components of the incident velocity. The measured vertical restitution coefficient was plotted against the incident angle at incident velocities of 3.5, 5.0, 7.5 and 10.0 m/s in **Fig. 19**. Though the wide distribution of the measured points is meaningful and significant, simple arithmetic means are given in **Fig. 20**, which shows the average decrease in the mean vertical restitution coefficient with the incident angle and the negligible dependence on incident velocity. It is important to note that the frequency of the occurrence of the vertical restitution coefficient being larger than unity increased with the decreasing incident angle. This fact is essential in the development of ice particle saltation since the vertical restitution coefficient above unity implies that the rebound particle acquires a larger vertical speed than before the impact and that the particle can get into a higher level where a stronger wind is blowing.

**Fig. 21** gives each value of the vertical restitution coefficient plotted against the incident velocity at the incident angles of 10, 20 and 30 degrees. **Fig. 22** gives their arithmetic means. As noted in Figs. 19 and 20, the velocity dependence is not important in the velocity range of the present study.

In **Figs. 23, 24, 25 and 26**, histograms of the vertical restitution coefficient at given

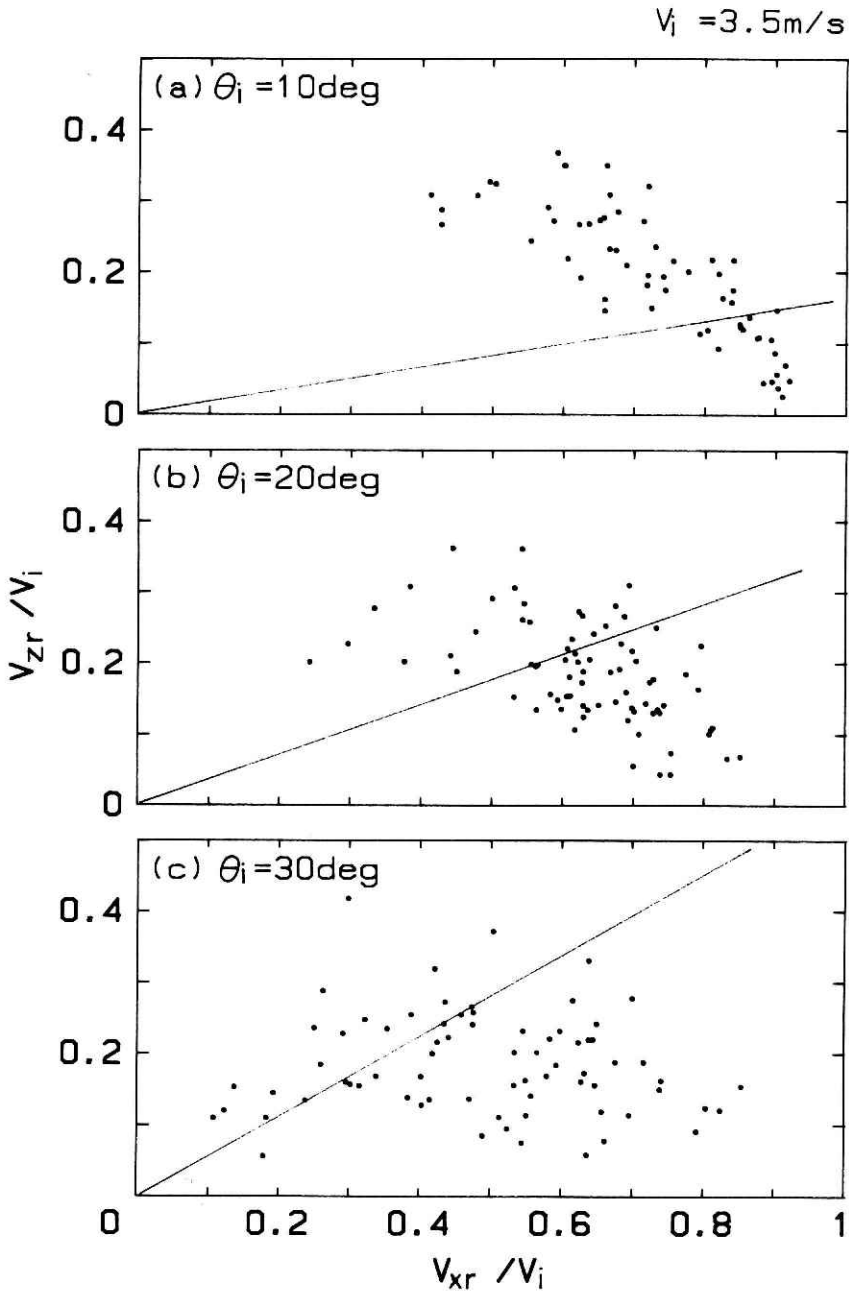


**Fig. 15** Relation between vertical and horizontal components of the rebound velocity normalized by the incident velocity. Incident angle: (a) 10 degrees, (b) 20 degrees, (c) 30 degrees. Incident velocity is 3.5 m/s. The straight line shown in each figure gives the rebound velocity vector with the identical velocity and angle of the incident velocity vector.

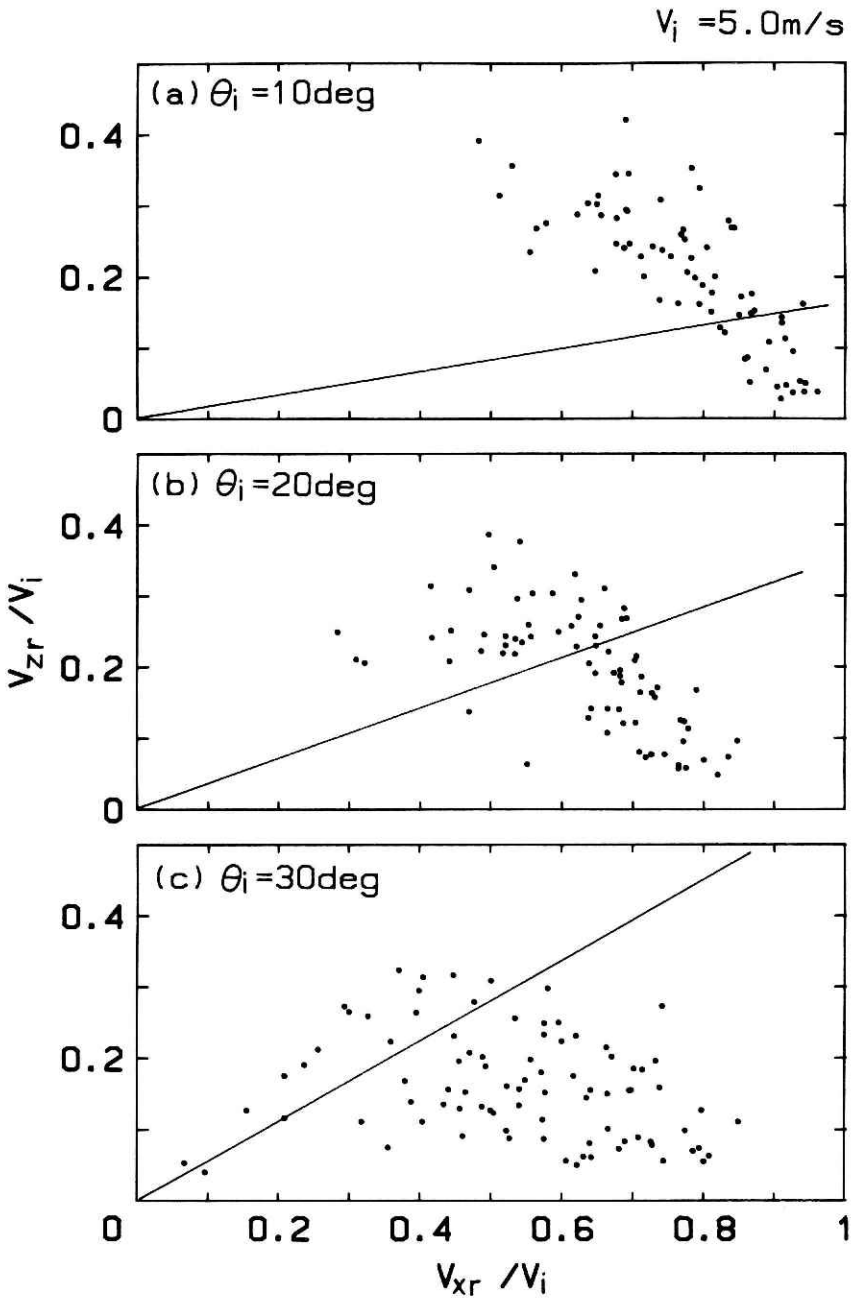


Fig. 16 Same as in Fig. 15 but for the incident velocity of 5.0 m/s.

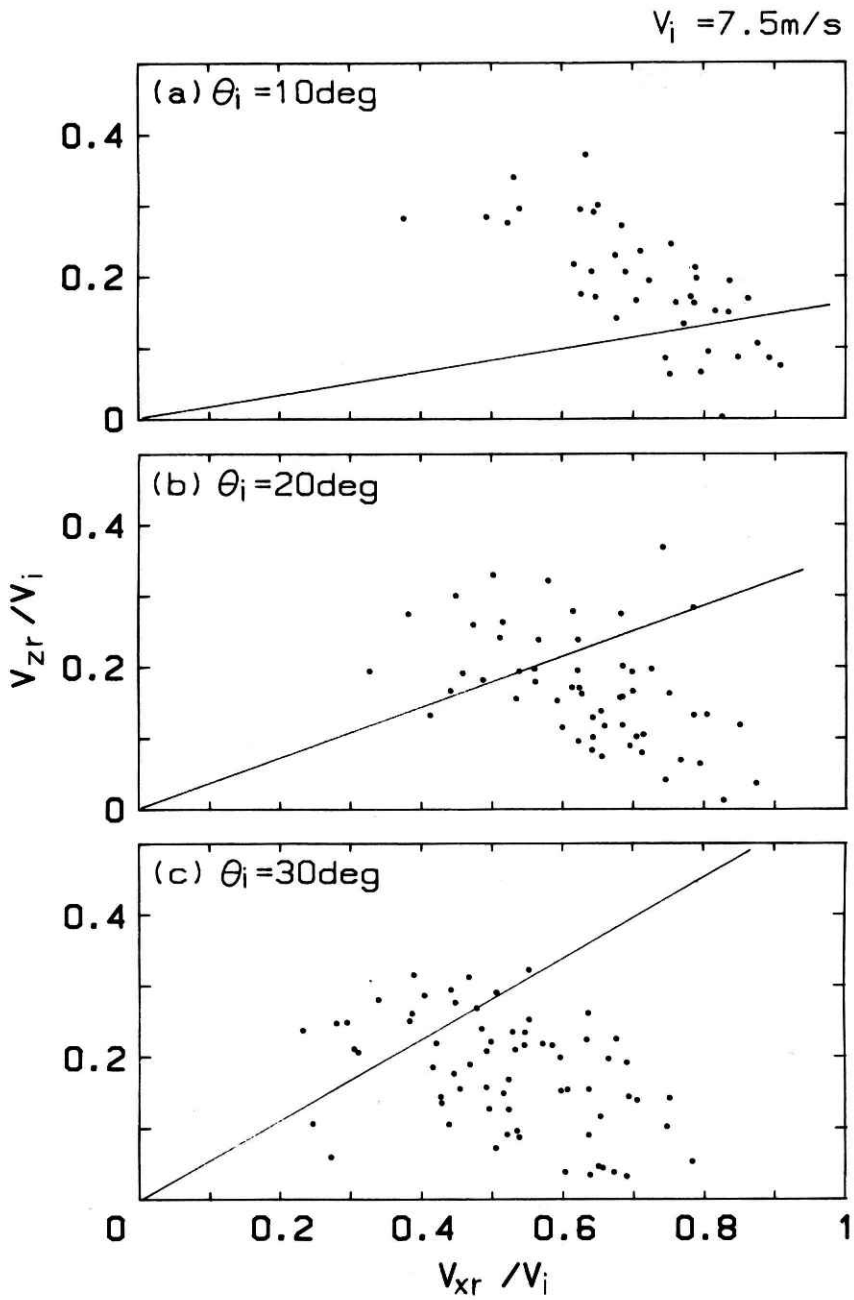


Fig. 17 Same as in Fig. 15 but for the incident velocity of 7.5 m/s.

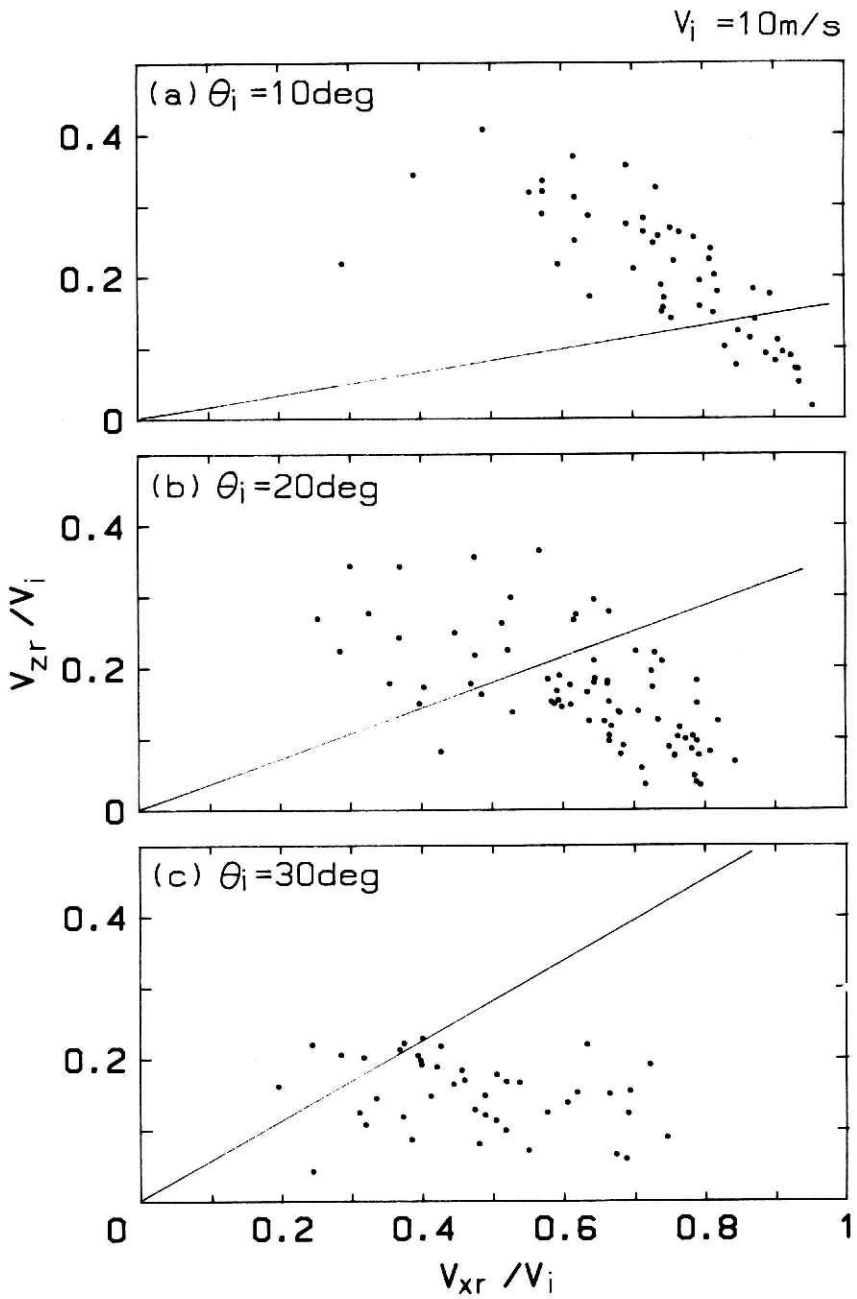


Fig. 18 Same as in Fig. 15 but for the incident velocity of 10 m/s.

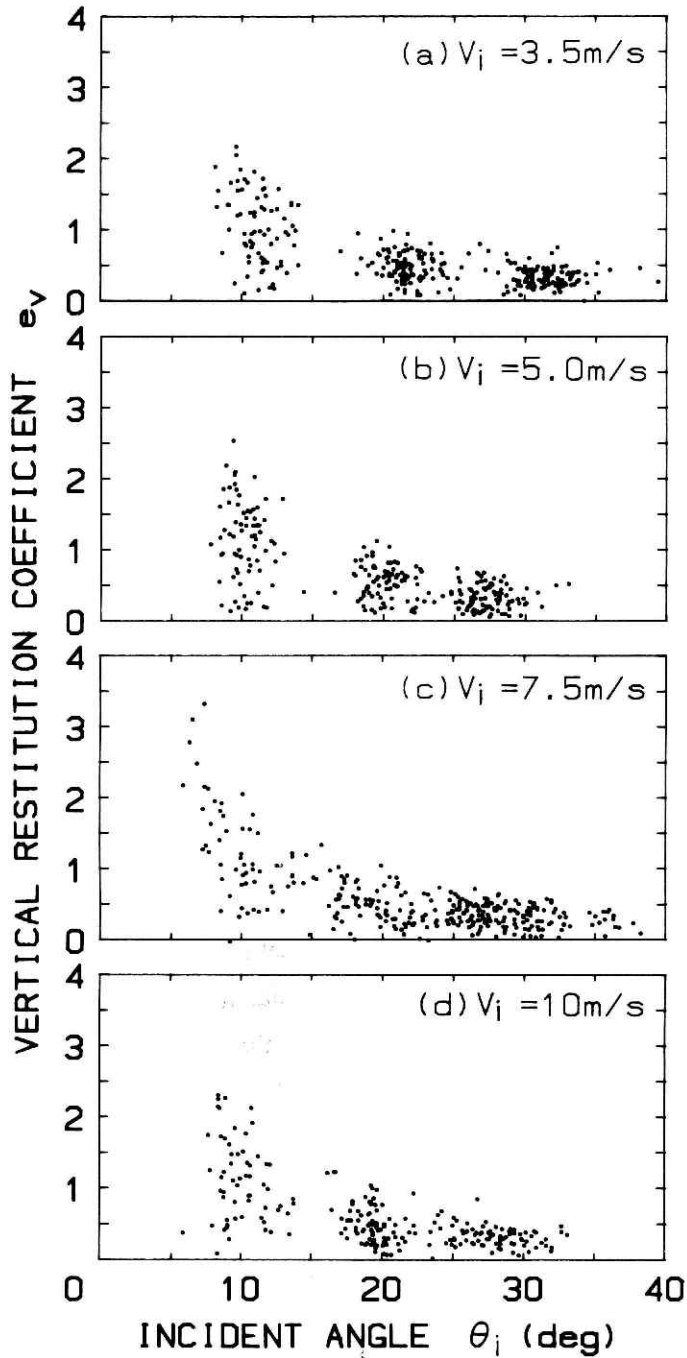


Fig. 19 Vertical restitution coefficient plotted against the incident angle. Incident velocity : (a) 3.5 m/s, (b) 5.0 m/s, (c) 7.5 m/s, (d) 10 m/s.

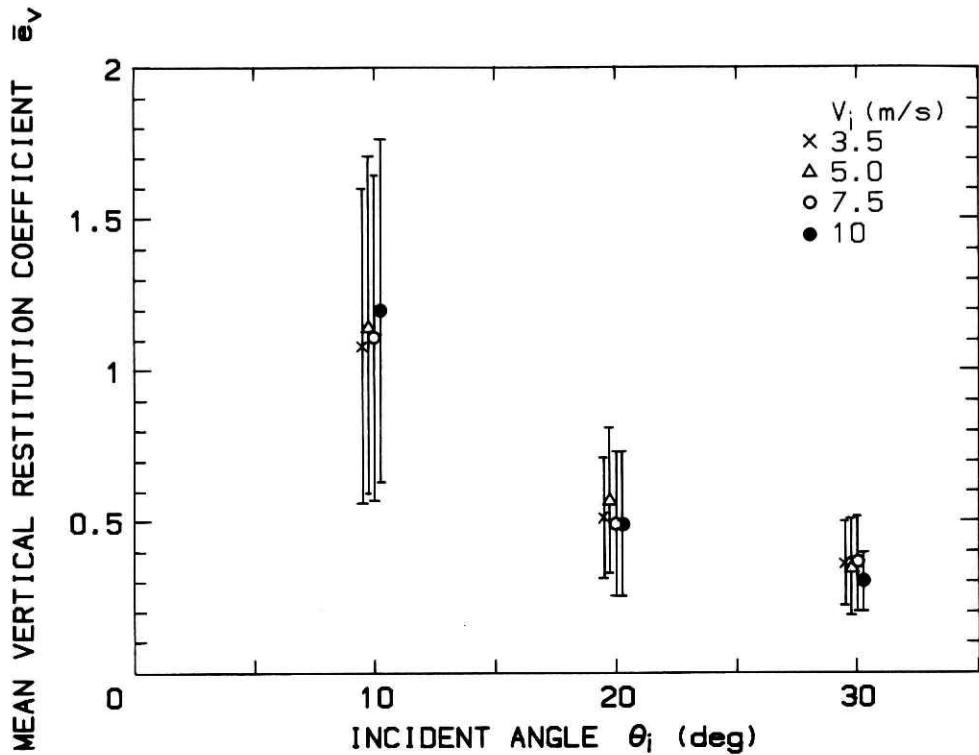


Fig. 20 Arithmetic means of vertical restitution coefficient plotted against the incident angles. Bars show the standard deviations.

incident angles and velocities are shown. It is apparent that larger coefficients than unity frequently appear at smaller incident angles. Similar results can be obtained from a simple computation of an ideal collision assuming that impact and bed particles are identical spheres, that the impact is smooth, and that the bed particles do not move (Fig. 27). The rebound velocity vector can be given by

$$V_r = V_i - (1 + e)(V_i \cdot n)n, \tag{3}$$

where  $V_i$ ,  $n$  and  $e$  are the incident velocity vector, unit vector normal to the particle surface, and restitution coefficient, respectively. The calculated probability of the occurrence of the vertical restitution coefficient for  $\theta_i=10$  degrees and  $e=0.8$  (after Araoka and Maeno, 1978) is shown in Fig. 28. The general characteristics are almost similar to those shown in Figs. 23-26. However, the magnitude of  $e_v$  appearing at each impact is much larger and amounts to one as large as 4.5. The unrealistic result is

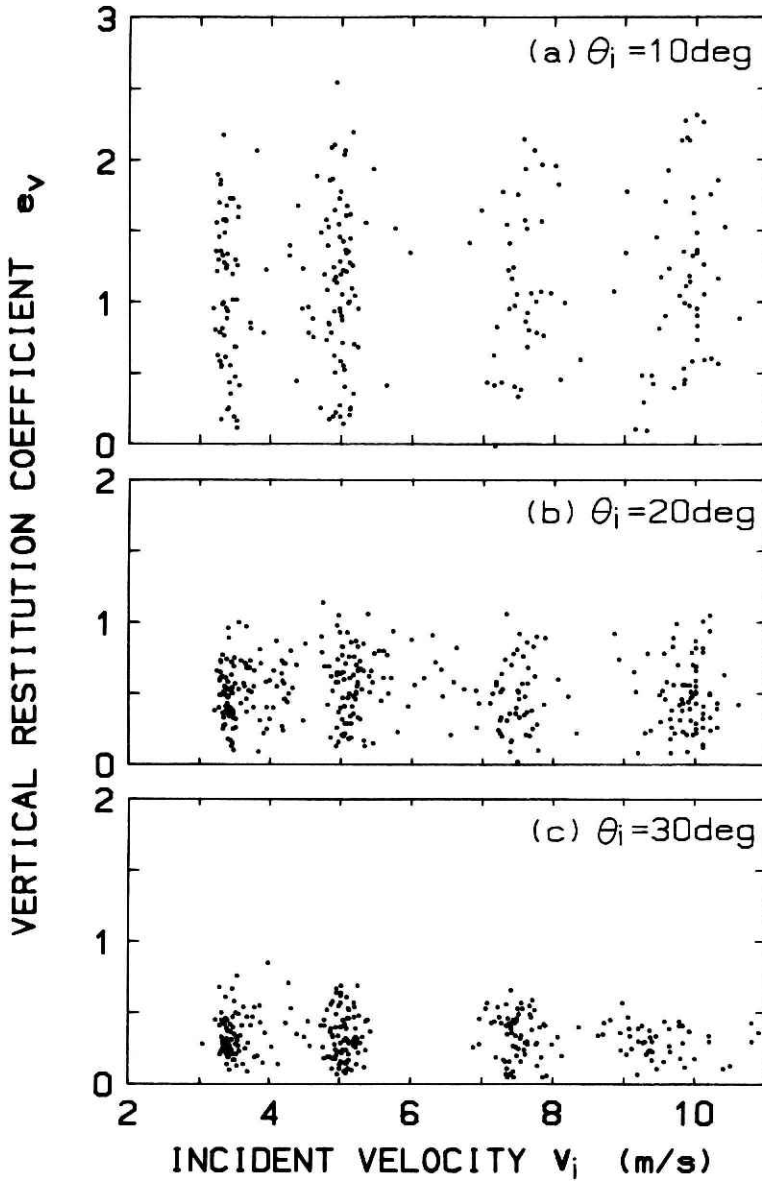


Fig. 21 Vertical restitution coefficient plotted against the incident velocity. Incident angle : (a) 10 degrees, (b) 20 degrees, (c) 30 degrees.

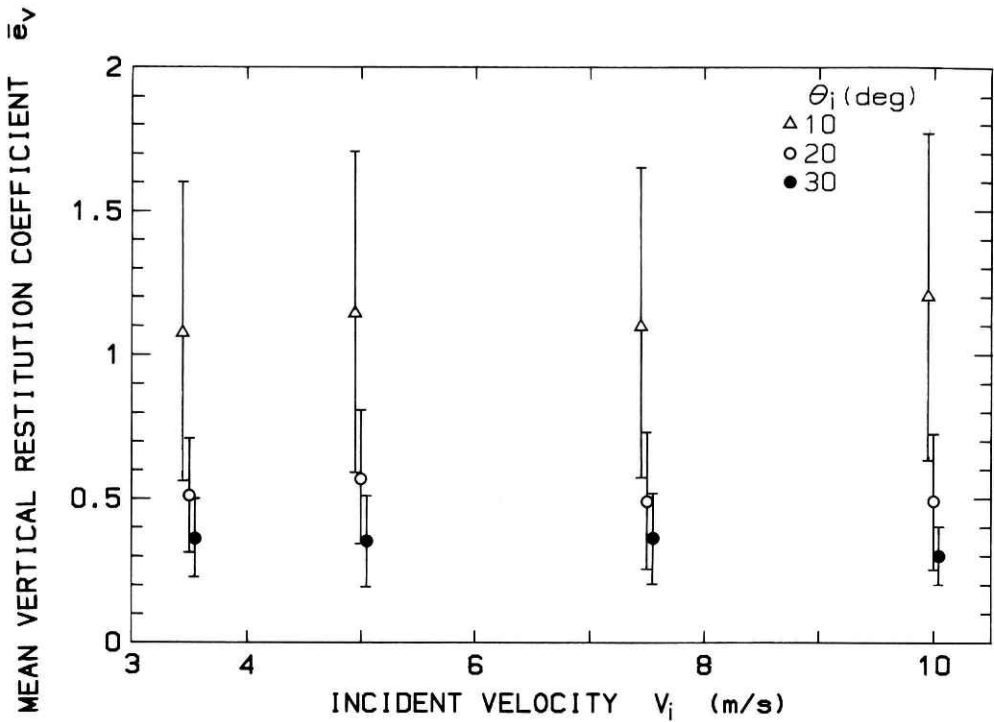


Fig. 22 Arithmetic means of vertical restitution coefficient plotted against the incident velocities. Bars show the standard deviations.

attributable to the physically improbable assumption of the interaction of bed particles, and implies the importance of the experimental measurements.

### 2.3 Determination of splash function

The splash function describing the impact process depends on various parameters such as the incident velocity and angle, mass or diameter of the impact particle, temperature, humidity, and others. In our experiment, however, the variables are only incident velocity and angle, and other variables were kept constant. Then the splash function,  $S(e_v, e_h, n_e; \theta_i, V_i)$ , can be defined as the function which gives the probability of  $e_v$ ,  $e_h$  or  $n_e$  at each impact as a function of  $\theta_i$  and  $V_i$ . We need the following three splash functions:  $S_v(e_v; \theta_i, V_i)$ ,  $S_h(e_h; \theta_i, V_i)$  and  $S_e(n_e; \theta_i, V_i)$  to describe completely the splash process. However, as mentioned earlier, only the splash function  $S_v$  is investigated in the present study.

The determination of the splash function  $S_v$  is straightforward to find a best fit function to the histograms shown in Figs. 23-26. It was found that the gamma distribu-

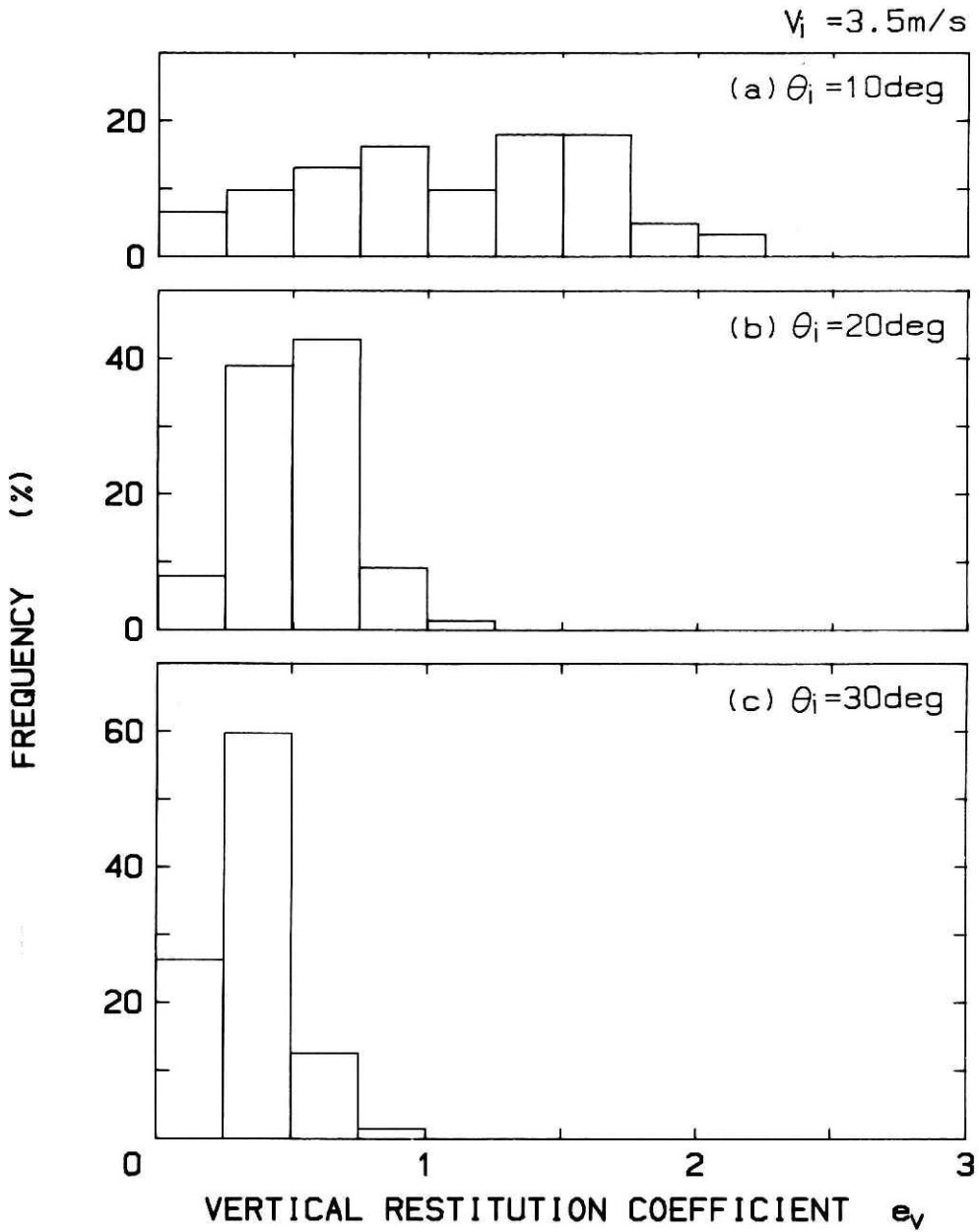


**Fig. 23** Histograms of the vertical restitution coefficient. Incident angle : (a) 10 degrees, (b) 20 degrees, (c) 30 degrees. Incident velocity is 3.5 m/s.

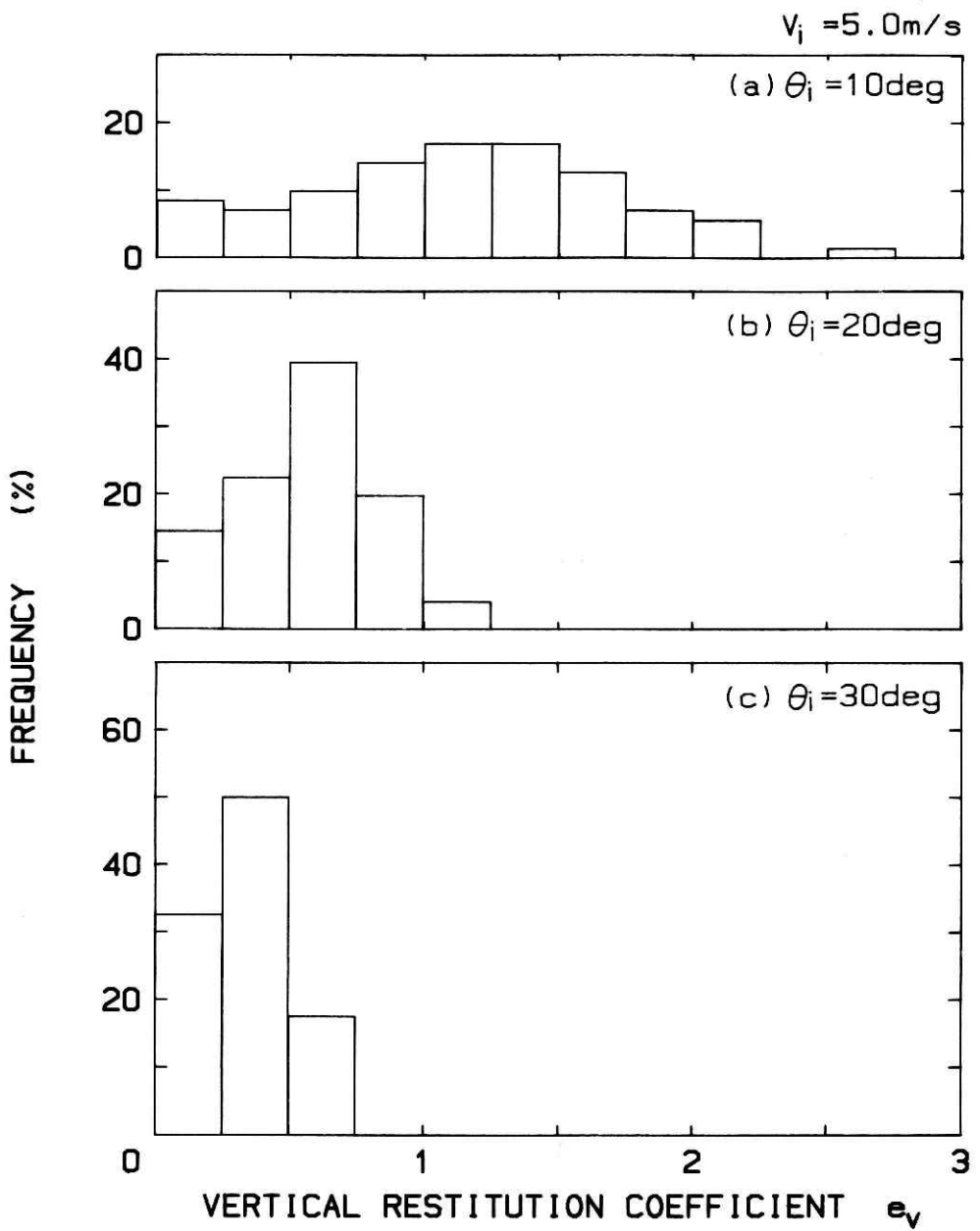


Fig. 24 Same as in Fig. 23 but for the incident velocity of 5.0 m/s.

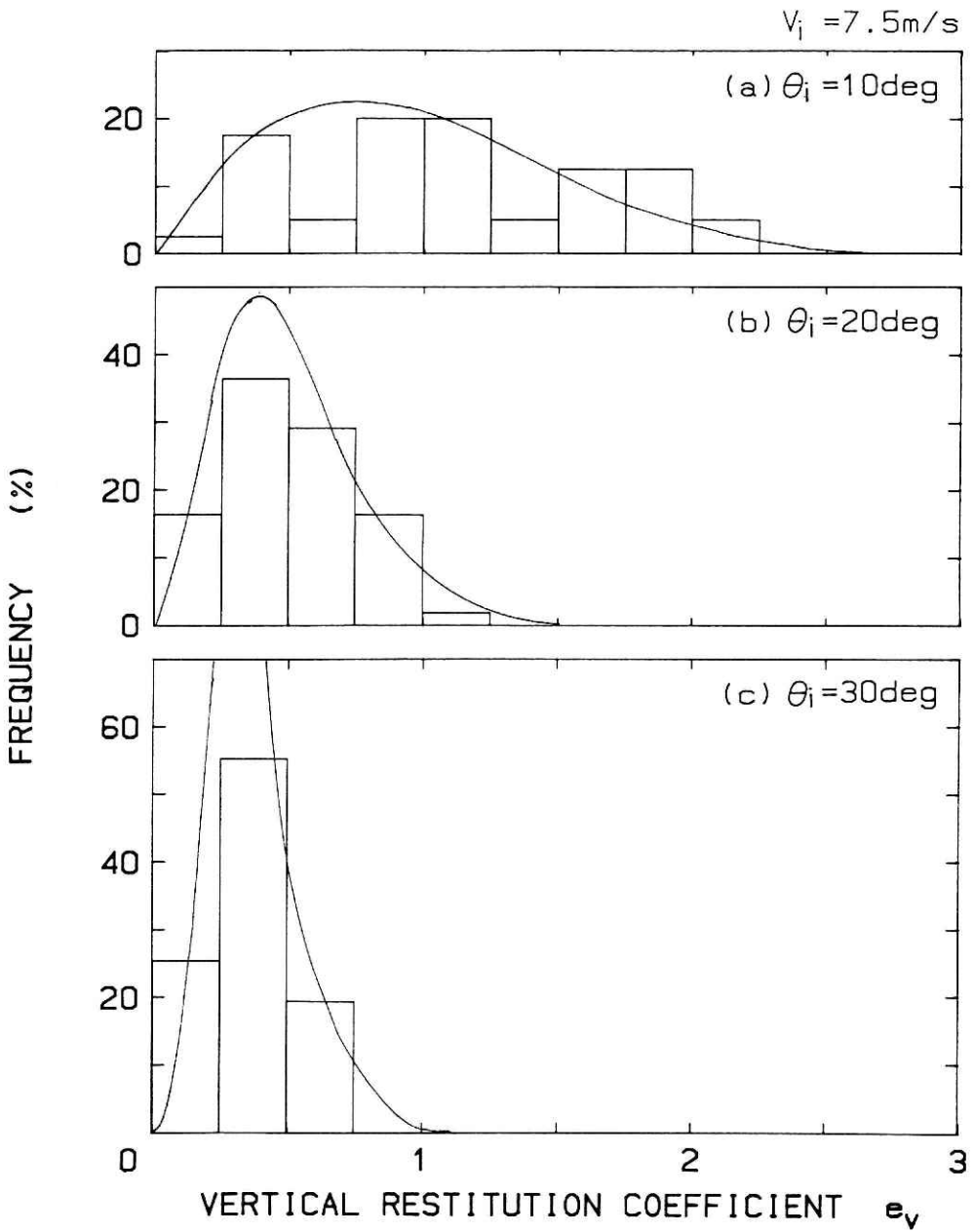


Fig. 25 Same as in Fig. 23 but for the incident velocity of 7.5 m/s.

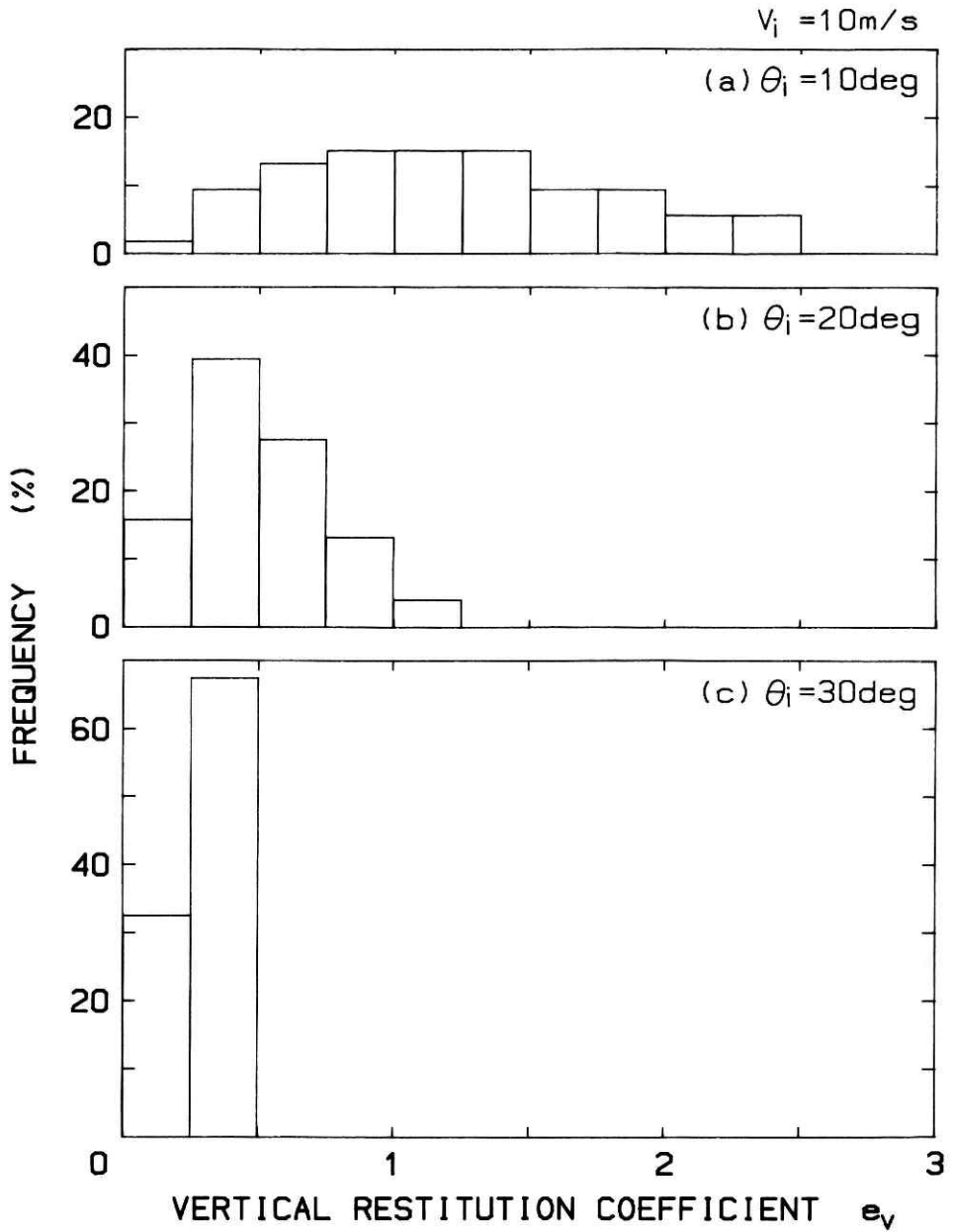
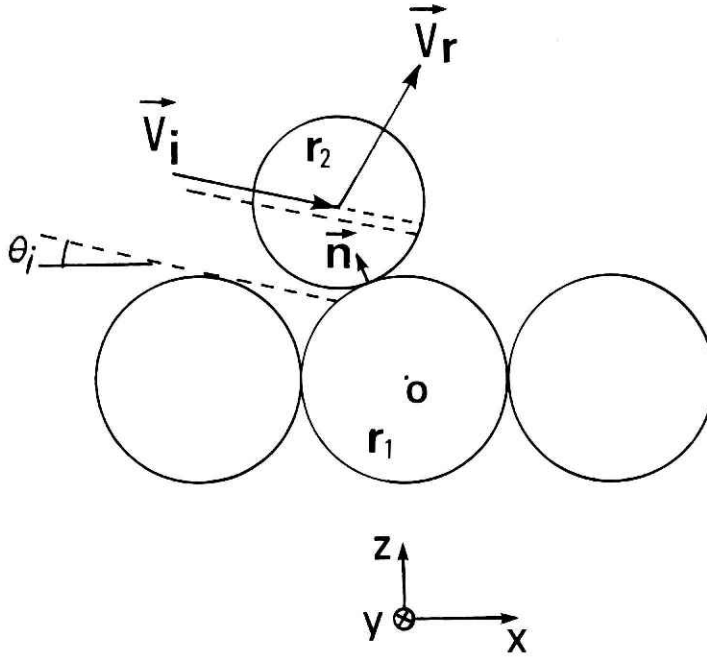


Fig. 26 Same as in Fig. 23 but for the incident velocity of 10 m/s.



**Fig. 27** Schematic description of the impact of a sphere of radius  $r_2$  on the bed composed of spheres of radii  $r_1$ .

tion is one of the best fit functions and some of the fitted curves are shown in the figures. The splash function is given by

$$S_v(e_v) = [1 / \beta \Gamma(\alpha)] (e_v / \beta)^{\alpha-1} \exp(-e_v / \beta), \quad (4)$$

where  $\Gamma(\alpha)$  is the gamma function, and  $\alpha$  and  $\beta$  are the constants called the shape and scale parameters, respectively. The constants are independent of the incident velocity as shown in **Fig. 29**, but they are dependent strongly on the incident angle as shown in **Fig. 30** and described as follows:

$$\alpha = 0.056 \theta_1 + 3.8 \quad (5)$$

and

$$\beta = 4.9 \theta_1^{-1.3}. \quad (6)$$

All the statistical data obtained are listed in **Table 1**.

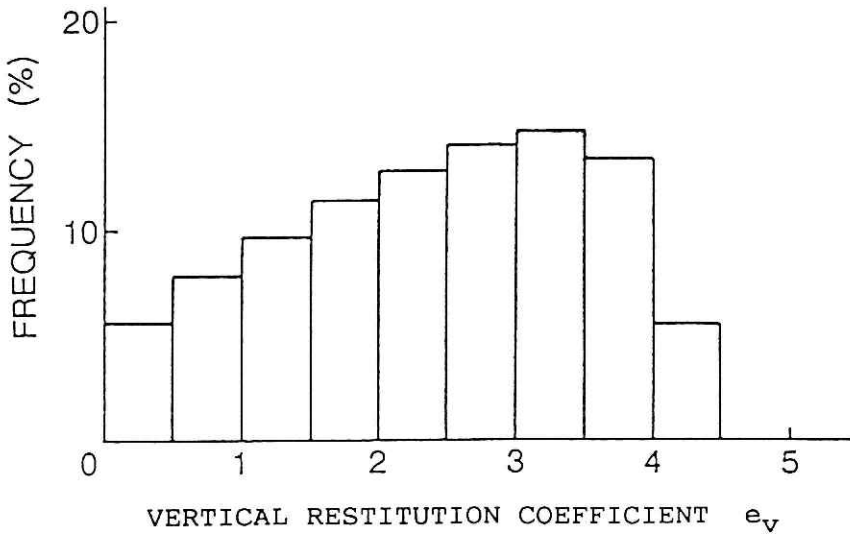


Fig. 28 Histogram of the calculated probability of the vertical restitution coefficient for the incident angle of 10 degrees. The restitution coefficient is assumed to be 0.8.

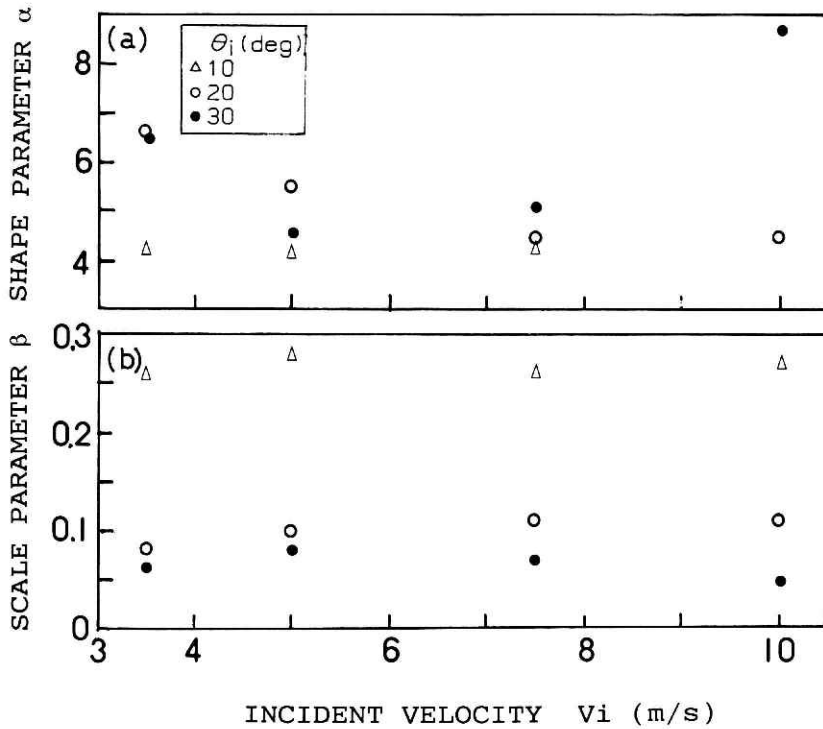


Fig. 29 Estimated shape (a) and scale (b) parameters of the gamma function plotted against the incident velocity. The parameters are estimated so as to fit to the experimental results.

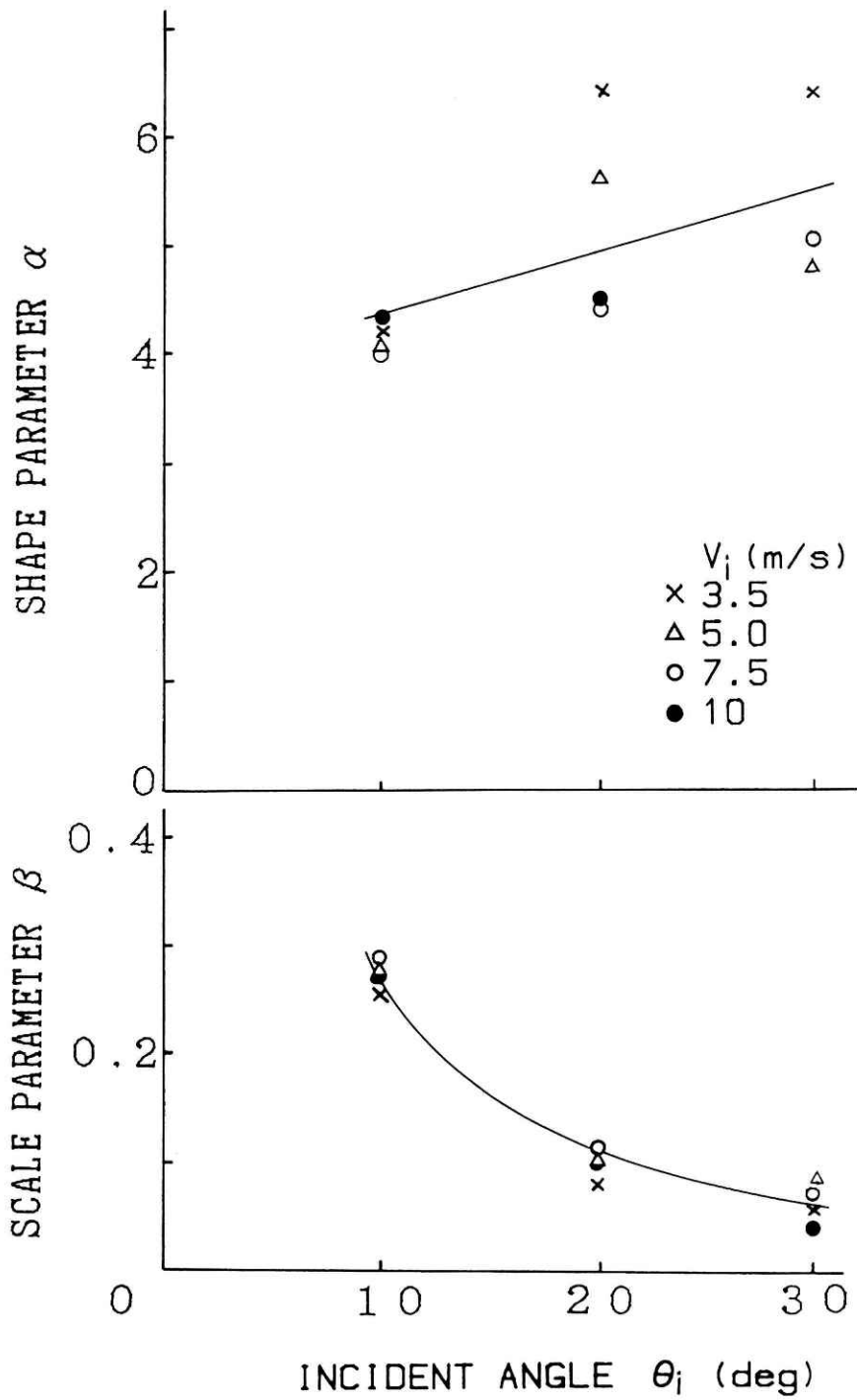


Fig. 30 Estimated shape (a) and scale (b) parameters of the gamma function plotted against the incident angle.

**Table 1** Statistical values of the splash experiments.

Vi (m/s)	$\theta_i$ (deg)	no. of data	e <sub>v</sub>											
			average	variance	S. D.	skewness	kurtosis	minimum	first quartile	median	third quartile	maximum	$\alpha$	$\beta$
3.5	10	61	1.08	0.28	0.52	0.023	2.07	0.14	0.65	1.03	1.51	2.20	4.2	0.26
	20	77	0.51	0.04	0.20	0.254	2.82	0.11	0.38	0.51	0.64	1.01	6.6	0.08
	30	72	0.36	0.02	0.14	0.607	3.17	0.11	0.25	0.33	0.46	0.78	6.5	0.06
5.0	10	71	1.15	0.32	0.56	0.045	2.42	0.17	0.75	1.19	1.56	2.57	4.2	0.28
	20	76	0.57	0.06	0.24	0.060	2.38	0.14	0.39	0.59	0.73	1.15	5.5	0.10
	30	86	0.35	0.03	0.16	0.413	2.26	0.08	0.21	0.33	0.47	0.71	4.5	0.08
7.5	10	40	1.11	0.29	0.54	0.168	2.18	0.00	0.76	1.05	1.57	2.17	4.2	0.26
	20	55	0.49	0.06	0.24	0.327	2.50	0.03	0.33	0.50	0.62	1.07	4.4	0.11
	30	67	0.36	0.03	0.16	-0.208	2.12	0.06	0.24	0.37	0.47	0.68	5.1	0.07
10	10	53	1.20	0.33	0.57	0.252	2.22	0.11	0.76	1.19	1.54	2.34	4.4	0.27
	20	76	0.49	0.06	0.24	0.514	2.60	0.10	0.31	0.47	0.61	1.07	4.4	0.11
	30	43	0.30	0.01	0.10	-0.288	2.13	0.08	0.24	0.32	0.39	0.48	8.7	0.04

### 3. Wind-tunnel experiments of ice particle saltation

In this chapter we describe wind-tunnel experiments of drifting or blowing snow with the ice particles used in the splash experiments. Although the ice particles are larger than snow particles usually observed in natural drifting snow, drifting snow actually occurs in the wind-tunnel experiments. We obtained results which are used in the comparison with the numerical calculation using the splash function determined in the preceding chapter.

#### 3.1 Apparatus and method

Drifting or blowing snow was produced in a cold wind-tunnel, whose schematic view is shown in **Fig. 31**. The working length of the wind-tunnel is 8.0 m and its cross section is 50 cm × 50 cm. The underlying snow was prepared from similar ice particles which were used in the splash experiments described in the preceding chapter. The thickness and length of the snow bed were 2.5 cm and 2.5 m, respectively, and its surface was prepared to be as smooth as possible.

To initiate the drifting snow, the seeding of ice particles was necessary. The seed ice particles were supplied with a seeding device. It was located under the windward end of the working section. The seeding device was composed of a motor, a decelerator and a container of ice particles. The bottom of the container was lifted up by the motor and decelerator. Consequently, ice particles in the container were pushed into the wind-tunnel. The most important advantage of this method was that steady drifting snow was maintained without destroying the intrinsic wind structure.

The temperature of the wind-tunnel could be varied between 0 and -30 °C, but the experiments for ice particle saltation were conducted at -18 °C in order to prevent rapid

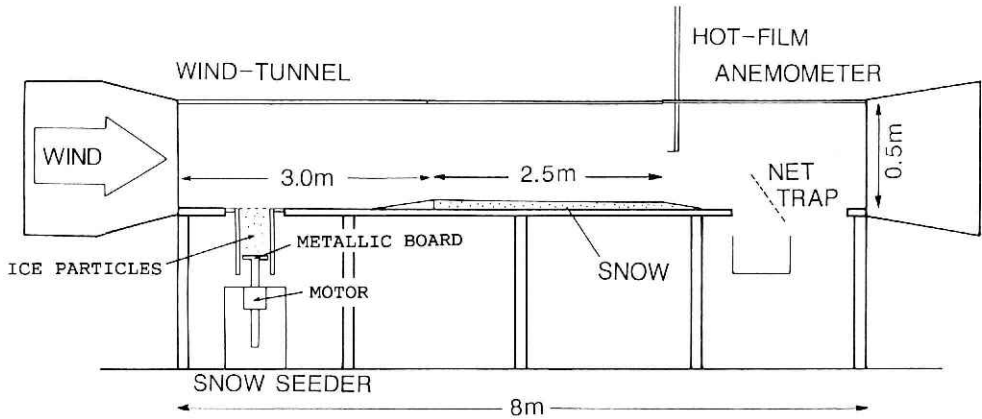


**Fig. 31** Schematic diagram of the wind-tunnel.

adhesion due to the sintering between ice particles during the experiment.

The wind velocity was measured with a hot-film type anemometer. It was found that a turbulent boundary layer of about 10 cm in thickness was steadily being formed over the snow surface.

A side view of the motion of the ice particles was taken with a video camera, 60 frames per second with the exposure time of 1/60 s or 1/1000 s.

### 3.2 Results of wind-tunnel experiments

It is known that the particle size in natural drifting and blowing snow is usually less than about 1 mm in diameter. The size of the particles used in the present wind-tunnel experiments (2.8 mm in average diameter) was much larger than that of natural drifting snow particles. In spite of this, the creep and saltation of ice particles were observed to take place in the wind-tunnel experiments.

**Photo 3 (a)** and **(b)** show trajectories and positions of ice particles in motion in the wind-tunnel experiment, respectively. In the figures the mean wind velocity at the middle height of the wind tunnel is 7.0 m/s. The direction of the particle movement is from right to left in the pictures. The exposure times for Photo 3 (a) and (b) are 1/60 s and 1/1000 s, respectively. The underlying snow surface, actually the ice particle bed, appears as a thick white horizontal belt in each photograph. White bars and points are ice particles creeping or saltating on the snow surface.

Vertical distributions of the number flux and concentration of saltating particles were obtained from pictures such as in Photo 3 (a) and (b), respectively. In Photo 3 (a), a line was drawn perpendicular to the snow surface. The number of ice particles crossing

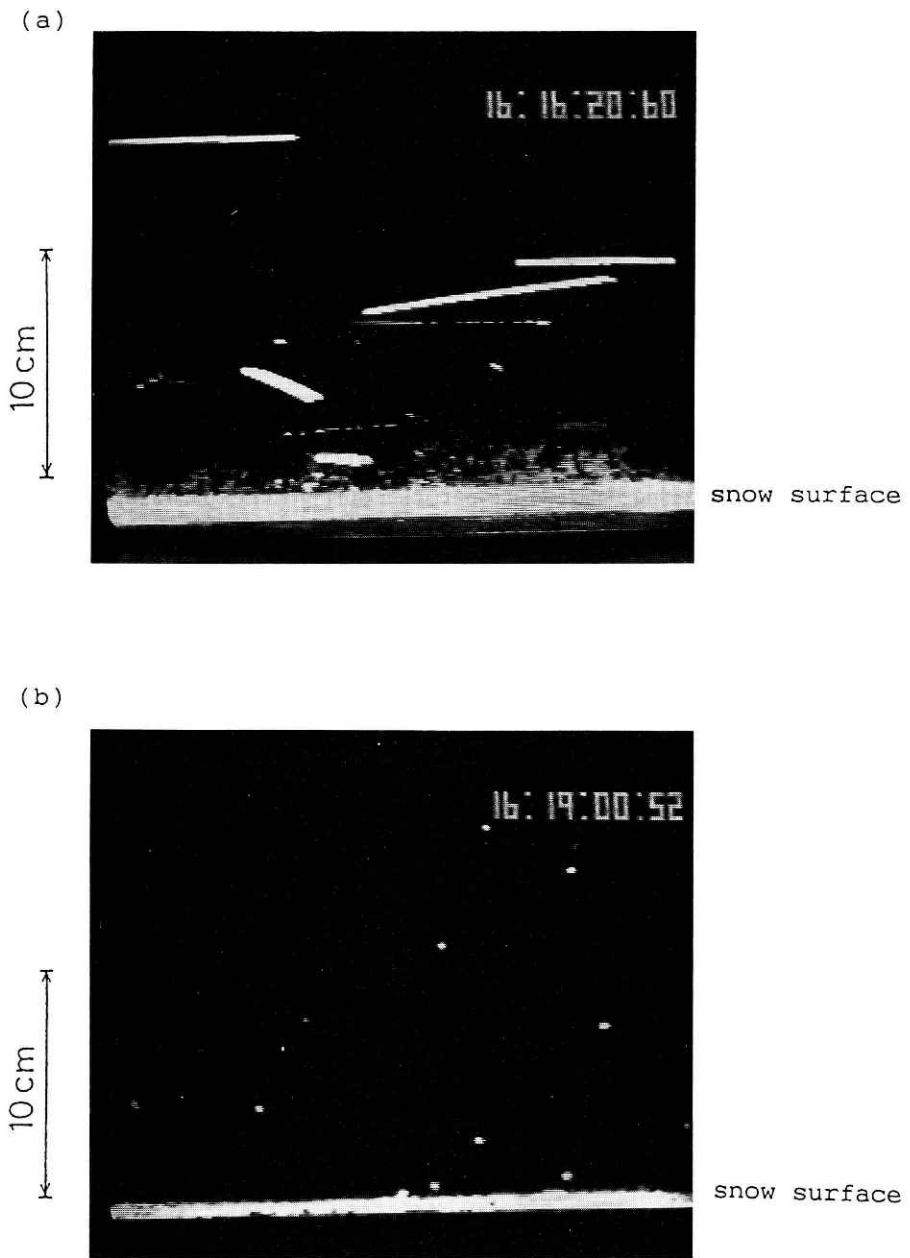


**Photo 3** Photographs of video images taken under the exposure time of 1/60 second (a) and 1/1000 second (b).

the line was counted in each height range, and it was divided by the total number of particles crossing the line to give the relative number flux, as shown in **Fig. 32**. The number flux increases as it approaches the surface. At least 100 successive pictures were necessary to obtain a meaningful distribution. **Fig. 33** shows the relative particle concentration. Each value was obtained from pictures such as in Photo 3 (b) as a fraction of the number of particles appearing in a height range to the total number. The concentration decreased exponentially with an increase in height. The above results are in agreement with observations of characteristic natural blowing snow (Kobayashi, 1972).

#### 4. Numerical experiments of ice particle saltation and the comparison of the results

##### 4.1 Numerical experiments of ice particle saltation

The motion of a single ice particle in a steady wind can be described by the following equations :

$$dx/dt = u, \quad (7)$$

$$dz/dt = w, \quad (8)$$

$$du/dt = -(3/8)[\rho_a/(\rho_p r)]C_d \Delta v (u - U), \quad (9)$$

$$dw/dt = -(3/8)[\rho_a/(\rho_p r)]C_d \Delta v w - g, \quad (10)$$

where  $r$  is the particle radius,  $\rho_a$  and  $\rho_p$  are the densities of the air and particle, respectively,  $g$  is the acceleration of the gravity,  $U$  is the horizontal wind speed, and  $\Delta v$  is written as

$$\Delta v = [(u - U)^2 + w^2]^{1/2}; \quad (11)$$

$C_d$  is the drag coefficient and given as (Morsi and Alexander, 1972)

$$C_d = 24 / Re + 6 / (1 + Re^{1/2}) + 0.4, \quad (12)$$

where  $Re$  is the Reynolds number defined by

$$Re = 2r \Delta v / \nu, \quad (13)$$

and  $\nu$  is the kinematic viscosity of the air.

The mean wind speed  $U$  was assumed to be described by a logarithmic relation often

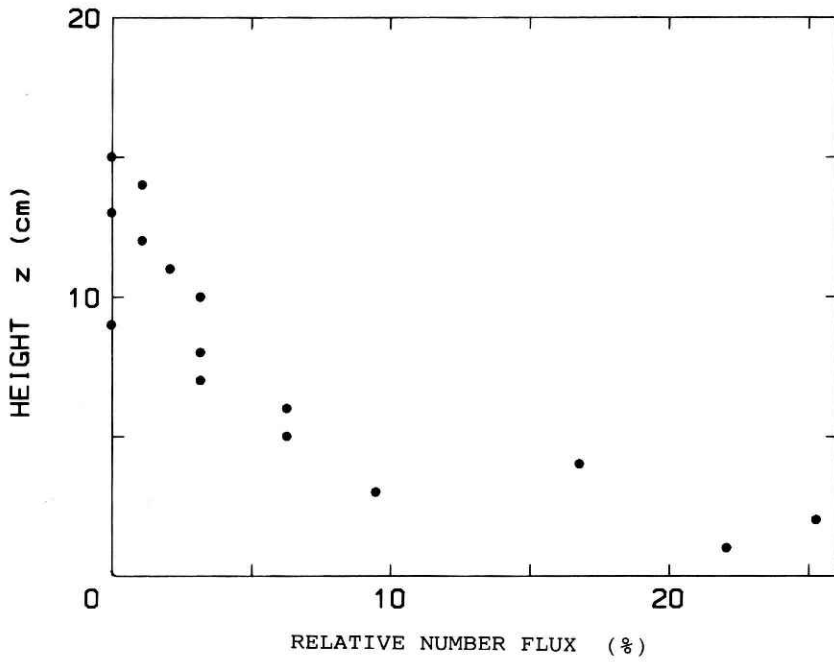


Fig. 32 Relation between the relative number flux and height at wind velocity 7.0 m/s.

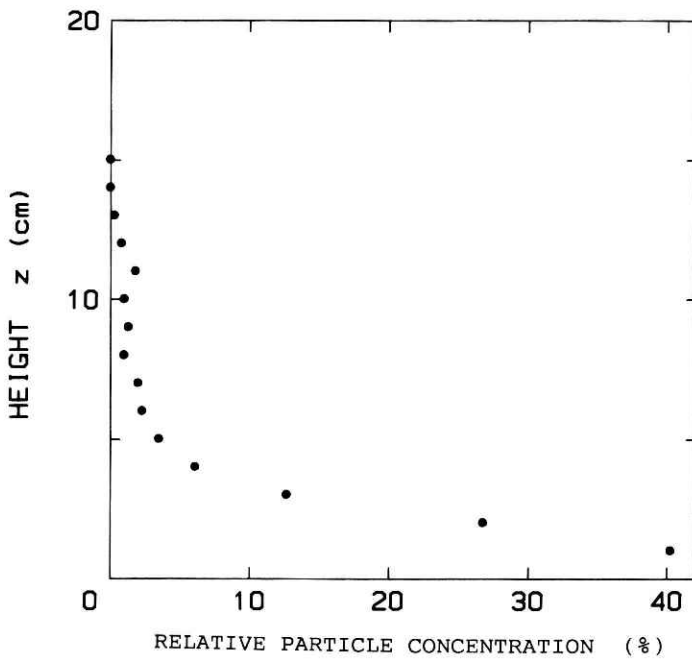


Fig. 33 Relation between the relative particle concentration and height at wind velocity 7.0 m/s.

found in a neutral condition:

$$U = (U_* / k) \ln(z / z_0), \quad (14)$$

where  $U_*$ ,  $k$  and  $z_0$  are the friction velocity, von Karman's constant (usually put as 0.4) and roughness parameter, respectively.

The kinematic process of the impact of the incident particle with the bed surface can be described by the following two relations:

$$V_{zr} = -e_v V_{zi} \quad (15)$$

and

$$V_{xr} = e_h V_{xi}, \quad (16)$$

in the probabilities given by the splash functions  $S_v(e_v)$  and  $S_h(e_h)$ , respectively. The production of ejected particles in the impact process may be taken into account by using the splash function  $S_e(n_e)$ . Furthermore, the momentum and energy must be conserved in the following manner:

$$m V_{zi} + I_z = m V_{zr}, \quad (17)$$

$$m V_{xi} + I_x = m V_{xr}, \quad (18)$$

and

$$m V_i^2 / 2 = m V_r^2 / 2 + E, \quad (19)$$

where  $m$  is the mass of the particle,  $I_z$  is the impulse and  $E$  is the energy dissipated by particle ejection and rearrangement as well as others.

**Fig. 34** shows the flow chart of the numerical calculation of saltation used in the present study. The motion of a single ice particle is initiated by giving an initial small vertical speed  $w_0$ . Its subsequent motion can be numerically calculated with the equations shown above. When a particle touches the snow surface, that is when it collides with the surface, the splash functions should be used to give the rebound velocity and angle after the collision.

In the present numerical experiment, the horizontal component of rebound velocities was set at zero, and the ejection of particles was not considered since the splash functions  $S_h(e_h)$  and  $S_e(n_e)$  have not been determined yet. **Fig. 35** is an example of these calcula-

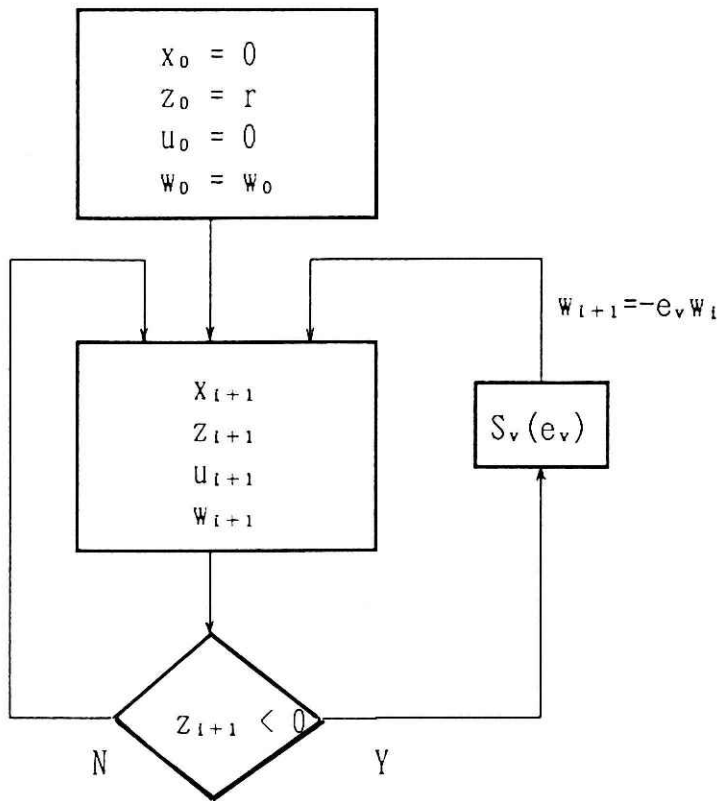


Fig. 34 Flow chart of the calculation of saltation.

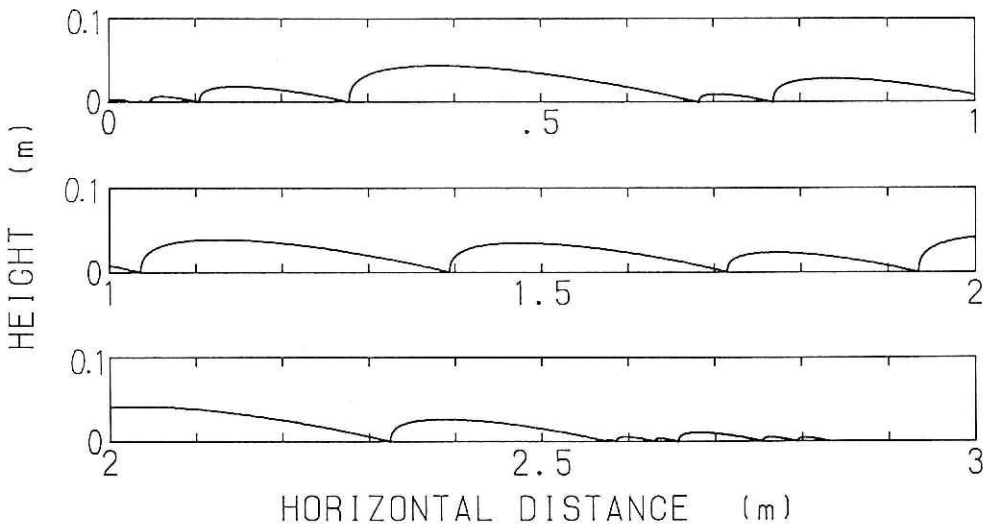


Fig. 35 Example of a calculated trajectory of a saltating particle.

tions for the particle radius of 1.4 mm and the initial vertical velocity of 0.3 m/s. The wind profile is as follows:  $U=7.0$  m/s at  $z=1$  m,  $U_* = 0.3$  m/s and  $z_0=0.1$  mm. The figure shows a realistic trajectory of a saltating ice particle in a statistical way specified by the splash function. From computed trajectories of saltating particles, various quantities in the saltation layer can be estimated, such as time variations and vertical profiles of particle concentration, flux, as well as others.

#### 4.2 Comparison of the results

Vertical distributions of the particle concentration were plotted in **Fig. 36** to compare the results of the wind-tunnel and numerical experiments. In both the diagrams, particle concentration means the number of particles appearing in a given layer and time interval, and accordingly its unit is arbitrary.

The important point in the figures is the exponential dependence of the particle concentration on the height. The dependence is characteristic of particle jumping in the saltation layer. The functional similarity of the results of the wind-tunnel and numerical experiments supports the basic validity of both the approaches.

### 5. Conclusions

The statistical saltation process was studied by measuring the collision characteristics of ice spheres on a granular bed composed of identical ice particles at a temperature of  $-18$  °C. Rebound velocities and angles of ice particles were measured as functions of incident velocity and angle.

- 1) The vertical restitution coefficient decreased with the increase in the incident angle due to the increasing interaction with lying particles.
- 2) The vertical restitution coefficient was almost independent of the incident velocity.
- 3) A single ice particle impact often produced ejected particles, and their number sometimes amounted to six.
- 4) The statistical behavior of the saltation process was described by a splash function  $S_v(e_v)$ , which refers to the vertical motion. The vertical splash function is only dependent on the incident angle and not on the incident velocities.
- 5) Ice particle saltation could be produced in a wind-tunnel by using the identical ice particles used in the splash experiment.
- 6) The measured vertical profiles of ice particle concentration were compared with those derived from the numerical calculation with use of the obtained splash function. The two results showed a reasonable agreement.

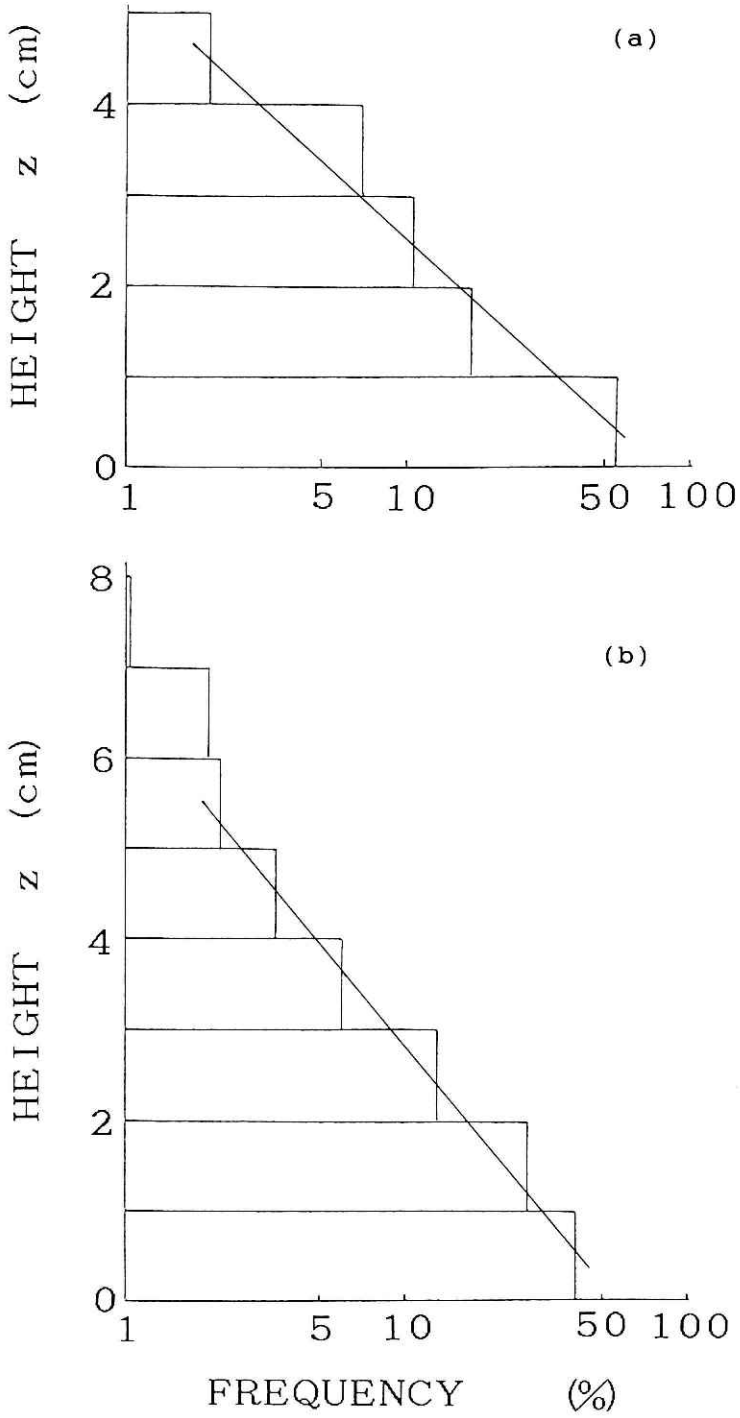


**Fig. 36** Vertical distribution of relative particle concentration. (a) numerical experiment, (b) wind-tunnel experiment.

### Acknowledgments

The authors wish to acknowledge Prof. D. Kobayashi and Dr. N. Ishikawa of the Institute of Low Temperature Science (I.L.T.S.), Hokkaido University, and Prof. K. Kikuchi of the Department of Geophysics, Hokkaido University, for their valuable discussion and comments. The authors are also grateful to Dr. H. Narita and Mr. M. Arakawa of I.L.T.S. for their helpful advice, cooperation and discussion throughout the study. Thanks are also due to Mr. J. Shimizu, Mr. M. Higa and Mr. S. Ishii for their experimental assistance. One of the authors (K. K.) is indebted to Dr. T. Kimura, the latest former Director, Director M. Higashiura and all other members of the Shinjo Branch of Snow and Ice Studies, National Research Institute for Earth Science and Disaster Prevention, for their kind encouragement while completing this work.

### References

- 1) Anderson, R.S. and Haff, P.K. (1988): Simulation of eolian saltation. *Science*, **241**, 820~823.
- 2) Araoka, K. and Maeno, N. (1978): Measurements of restitution coefficients of ice. *Low Temp. Sci., Ser. A*, **36**, 55~65.
- 3) Araoka, K. and Maeno, N. (1981): Dynamical behaviors of snow particles in the saltation layer. *Memoirs of National Institute of Polar Research*, **19**, 253~263.
- 4) Bagnold, R.A. (1941): *The physics of blown sand and desert dunes*. Methuen, London, 265 pp.
- 5) Budd, W.F., Dingle, W.R. and Radok, U. (1966): The Byrd snow drift project: outline and basic results. in M.J. Rubin (ed.), *Studies in Antarctic Meteorology*, American Geophysical Union, Antarctic Research Series, **9**, pp. 71~134.
- 6) Dyunin, A.K. (1954): Solid flux of snow-bearing air flow. National Research Council, Canada, Technical Translation 1102.
- 7) Dyunin, A.K. (1963): *Mechanics of drifting snow*. Novosibirsk, Siberian Branch of the USSR Academy of Sciences, Publishing House, 378 pp.
- 8) Irwin, P.A. (1983): Application of snow-simulation model tests to planning and design. *Proc. East Snow Conf.*, **28**, 118~130.
- 9) Kobayashi, D. (1972): Studies of snow transport in low-level drifting snow. *Contr. Low Temp. Sci., Ser. A*, No. **24**, 1~58.
- 10) Maeno, N., Naruse, R., Nishimura, K., Takei, I., Ebinuma, T., Kobayashi, S., Nishimura, H., Kaneda, Y. and Ishida, T. (1985): Wind-tunnel experiments on blowing snow. *Ann. Glaciol.*, **6**, 63~68.
- 11) Mitha, S., Tran, M.Q., Werner, B.T., and Haff, P.K. (1986): The grain-bed impact process in aeolian saltation. *Acta Mechanica*, **63**, 267~278.
- 12) Morsi, S.A. and Alexander, A.J. (1972): An investigation of particle trajectories in two phase flow systems. *J. Fluid Mech.*, **55**, 193~208.
- 13) Pomeroy, J.W. and Male, D.H. (1986): Physical modelling of blowing snow for agricultural production. *Proc. Symp. Snow Management for Agriculture* (edited by H. Steppuhn and others.), 73~108.
- 14) Uematsu, T., Kaneda, Y., Takeuchi, K., Nakata, T. and Yukumi, M. (1989): Numerical simulation of snowdrift development. *Ann. Glaciol.*, **13**, 265~268.
- 15) Willetts, B.B. and Rice, M.A. (1986): Collisions in aeolian saltation. *Acta Mechanica*, **63**, 255~265.
- 16) Wipperman, F.K. and Gross, G. (1985): The wind-induced shaping and migration of an isolated dune. A numerical experiment. *Boundary-Layer Meteorol.*, **36**, 319~334.

(Accepted : 29 August, 1994)

## 吹雪における粒子跳躍動力学の研究

小杉健二\*・西村浩一\*\*・前野紀一\*\*

\*防災科学技術研究所 新庄雪氷防災研究支所 雪氷防災第二研究室 科学技術特別研究員

\*\*北海道大学低温科学研究所

### 要 旨

跳躍運動は吹雪における雪粒子の輸送の最も基本的な過程である。統計的跳躍運動過程を、氷球(直径 2.8 mm)と、同じ粒子で形成される粒子層との衝突特性を調べることで研究した。温度 $-18^{\circ}\text{C}$ の下で氷粒子の反発の速度と角度を入射の速度と角度の関数として測定し、反発速度の鉛直成分と入射速度の鉛直成分の比として定義される鉛直反発係数( $e_v$ )を算出した。

平均の鉛直反発係数は、入射角度の増大とともに、粒子層の粒子との相互作用が強まることにより減少した。一方、それは入射速度にはほとんど依存しなかった。ひとつの氷粒子の衝突はしばしば他の氷粒子をはじき出し、その数は時として6個におよんだ。

跳躍過程の統計的ふるまいは、スプラッシュ関数  $S_v(e_v)$ ,  $S_h(e_h)$  および  $S_e(n_e)$  により表現される。ここで、 $e_v$ ,  $e_h$  および  $n_e$  はそれぞれ鉛直反発係数、水平反発係数およびはじき出された粒子数である。それぞれのスプラッシュ関数は、それぞれの物理量の出現確率を表現する。本研究では、スプラッシュ関数  $S_v(e_v)$  が次のように求められた。

$$S_v(e_v; \theta_i, V_i) = [1/\beta\Gamma(\alpha)](e_v/\beta)^{\alpha-1}\exp(-e_v/\beta)$$

ここで、 $\theta_i$  と  $V_i$  はそれぞれ入射角度と入射速度、 $\Gamma(\alpha)$  はガンマ関数、 $\alpha$  は形状母数 ( $\alpha=0.056\theta_i+3.8$ )、そして  $\beta$  は尺度母数 ( $\beta=4.9\theta_i^{-1.3}$ ) である。この結果は、鉛直運動のスプラッシュ関数は入射角度のみに依存し、本研究の範囲(3.5–10 m/s)では入射速度に依存しないことを示す。

跳躍運動の風洞実験と数値実験が行われ、氷粒子数密度の鉛直分布が求められた。風洞実験では、衝突実験で用いられた氷粒子と同じものが使用された。数値実験では、衝突実験から導かれたスプラッシュ関数が跳躍氷粒子の反発速度の決定に応用された。跳躍運動のこれらふたつの実験結果はともに、高さの増大とともに粒子数密度が指数関数的に減少することを示した。この結果は跳躍層における跳躍運動による質量輸送を特徴づけるものである。

キーワード：吹雪 (drifting snow), 跳躍運動 (saltation), 反発係数 (restitution coefficient), 衝突実験 (impact experiments), スプラッシュ関数 (splash function)